Tellus SERIES B CHEMICAL AND PHYSICAL METEOROLOGY
PUBLISHED BY THE INTERNATIONAL METEOROLOGICAL INSTITUTE IN STOCKHOLM

Tellus (2009), 61B, 500–535
Printed in Singapore. All rights reserved

TELLUS

The tropospheric cycle of H_2: a critical review

By D. H. EHHALT and F. ROHRER*, *Forschungszentrum Jülich, Institut ICG-2: Troposphäre, 52425 Jülich, Germany*

(Manuscript received 14 July 2008; in final form 22 December 2008)

ABSTRACT

The literature on the distribution, budget and isotope content of molecular hydrogen (H_2) in the troposphere is critically reviewed. The global distribution of H_2 is reasonably well established and is relatively uniform. The surface measurements exhibit a weak latitudinal gradient with 3% higher concentrations in the Southern Hemisphere and seasonal variations that maximize in arctic latitudes and the interior of continents with peak-to-peak amplitudes up to 10%. There is no evidence for a continuous long-term trend, but older data suggest a reversal of the interhemispheric gradient in the late 1970s, and an increase in the deuterium content of H_2 in the Northern Hemisphere from 80‰ standard mean ocean water (SMOW) in the 1970s to 130‰ today. The current budget analyses can be divided in two classes: bottom up, in which the source and sink terms are estimated separately based on emission factors and turnovers of precursors and on global integration of regional loss rates, respectively. That category includes the analyses by 3-D models and furnishes tropospheric turnovers around 75 Tg H_2 yr^{-1}. The other approach, referred to as top down, relies on inverse modelling or analysis of the deuterium budget of tropospheric H_2. These provide a global turnover of about 105 Tg H_2 yr^{-1}. The difference is due to a much larger sink strength by soil uptake and a much larger H_2 production from the photochemical oxidation of volatile organic compounds (VOC) in the case of the top down approaches. The balance of evidence seems to favour the lower estimates—mainly due to the constraint placed by the global CO budget on the H_2 production from VOC. An update of the major source and sink terms yields: fossil fuel use 11 ± 4 Tg H_2 yr^{-1}; biomass burning (including bio-fuel) 15 ± 6 Tg H_2 yr^{-1}; nitrogen fixation (ocean) 6 ± 3 Tg H_2 yr^{-1}; nitrogen fixation (land) 3 ± 2 Tg H_2 yr^{-1}; photochemical production from CH_4 23 ± 8 Tg H_2 yr^{-1} and photochemical production from other VOC 18 ± 7 Tg H_2 yr^{-1}. The loss through reaction of H_2 with OH is 19 ± 5 Tg H_2 yr^{-1}, and soil uptake 60^{+30}_{-20} Tg H_2 yr^{-1}. All these rates are well within the ranges of the corresponding bottom up estimates in the literature. The total loss of 79 Tg H_2 yr^{-1} combined with a tropospheric burden of 155 Tg H_2 yields a tropospheric H_2 lifetime of 2 yr. Besides these major sources of H_2, there are a number of minor ones with source strengths <1 Tg H_2 yr^{-1}. Rough estimates for these are also given.

1. Introduction

The presence of molecular hydrogen (H_2) in the atmosphere has been recognized for a long-time—the first reliable measurements being reported by Paneth (1937). Its major sources and sinks, however, were not identified before the early 1970s (Schmidt, 1974). Currently, H_2 has an average tropospheric mixing ratio of about 530 ppb (Novelli et al., 1999). It is, thus, the second most abundant oxidizable trace gas in the troposphere. Moreover, H_2 has a large turnover in the troposphere. The estimated total loss of 79 Tg yr^{-1} corresponds to 39 Tmol yr^{-1} in molar units, a molecular turnover that is second only to that of carbon monoxide (CO) but as large as that of methane (CH_4) (Ehhalt, 1999). After years of neglect, the tropospheric budget of H_2 has gained renewed interest during the last decade, partly triggered by the prospect of a future H_2 fuel economy (Prather, 2003, Schultz et al., 2003, Tromp et al., 2003) but mostly on its own merit, as a significant element of tropospheric and stratospheric chemistry and a means of additional insight into the trace gas cycles to which it is coupled, notably that of CO.

There is one feature that makes the tropospheric cycle of H_2 particularly interesting: troposheric H_2 is removed predominantly by soil uptake. This feature is unique among the oxidizable trace gases. It has the consequence that the sink strength for H_2 is hemispherically asymmetric—much larger in the Northern Hemisphere owing to the larger continental area. As a result, the H_2 mixing ratios observed in the Northern Hemisphere are lower than those in the Southern Hemisphere (Khalil and Rasmussen, 1990; Novelli et al., 1999; Simmonds et al., 2000), despite the fact that the known H_2 sources are located predominantly in the Northern Hemisphere.

The dominance of the soil sink has also made it more difficult to quantify the H_2 budget. In contrast to CH_4, whose tropospheric loss is essentially governed by the reaction with

*Correspondig author.
e-mail: f.rohrer@fz-juelich.de
DOI: 10.1111/j.1600-0889.2009.00416.x

hydroxyl radical (OH) and thus reasonably well established since the average tropospheric OH concentration is reasonably well determined empirically (Prinn et al., 1995), such a constraint is missing for H_2. As a consequence, the estimates of its tropospheric turnover have varied more widely than that of CH_4.

Over the past decade, there has been a considerable improvement in our knowledge of the temporal and spatial distribution of tropospheric H_2, largely due to the efforts of NOAA's Global Monitoring Division (GMD), formerly the Climate Modelling and Diagnostics Laboratory (CMDL). This improvement enabled the application of 3-D global Chemistry-Transport Models (CTM) to study the H_2 budget in much better temporal and spatial detail than hitherto possible and test it for consistency (Hauglustaine and Ehhalt, 2002; Sanderson et al., 2003; Price et al., 2007). At the same time, there were other, top down approaches, such as inverse modelling (Xiao et al., 2007) or the use of the deuterium budget of tropospheric H_2 (Rahn et al., 2003, Rhee et al., 2006a), to specifically determine the global uptake by soil. Some are still with conflicting results. It seems, therefore, worthwhile to critically review the tropospheric H_2 cycle, its sources and sinks, with particular emphasis on the recent literature. We include some of the older literature, however, to point out possible changes or trends.

2. The atmospheric abundance of H_2: spatial and temporal distributions

2.1. Global trends

The first reliable measurements of the tropospheric H_2 abundance were reported by Paneth (1937) as 0.5 ppm. They were made in 1923 by Schuftan at Höllriegelskreuth, an air liquefaction plant in southern Germany. This value was implicitly considered as globally applicable and was widely used up to the 1970s. It is, in fact, surprisingly close to today's globally averaged mixing ratio for tropospheric H_2 of 531 ± 6 ppb, derived by Novelli et al. (1999) (Unless stated differently, the errors quoted throughout the text refer to 1σ bounds).

The few subsequent surface measurements made at European locations up to 1970 by Glueckauf and Kitt (1957), Ehhalt et al. (1966) and Schmidt and Seiler (1970) were summarized by Schmidt (1974) (see also Schmidt and Wetter, 2002). Often subject to local pollution, they all gave variable results ranging from 400 to 1500 ppb and did not allow to deduce a reliable trend even when the then-existing shipboard and aircraft measurements were included (Surface mixing ratios of H_2 downwind of large cities or along highways easily exceed 1000 ppb till today). The determination of a trend became possible only after the installation of background stations. A first attempt was made by Khalil and Rasmussen (1990), who from late 1985 to early 1989 took weekly air samples at six clean air stations around the world for H_2 analysis. From these observations, they deduced an increase in tropospheric H_2 of $(0.6 \pm 0.1)\%$ yr^{-1}. They further speculated that the H_2 mixing ratio in pre-industrial times may have been as low as 200 ppb. There is, however, no direct evidence for the latter.

A real breakthrough came in the late 1980s when NOAA's GMD began to establish a global network of sampling stations for trace gas analysis. The sampling sites used for H_2 analysis are given in Novelli et al. (1999), who also describe sampling techniques, analytical procedure and calibration. These authors also present the time-series of the H_2 mixing ratios at numerous background stations—augmented by shipboard measurements. The current data are made available at the NOAA CMDL website (http://www.cmdl.noaa.gov). As an example, the series of monthly averaged H_2 mixing ratios at Mauna Loa, Hawaii is shown in Fig. 1. A closer look reveals a seasonal variation, substantial interannual variability and even periods of sustained change lasting up to 5 yr. But there is no apparent long-term trend. This is also true for the time-series in H_2 abundance at the other surface stations (Novelli et al., 1999; see also CMDL website). Thus, over the past two decades, a trend in the global troposperic H_2 abundance—if present at all—must have been quite small. We note, however, that over the shorter period 1991–1996, the data from the same stations indicated a global decrease of -2.3 ± 0.1 ppb yr^{-1} (Novelli et al., 1999). At about the same time, 1994–1998, Simmonds et al. (2000) deduced a trend of $+1.2 \pm 0.8$ ppb yr^{-1} for northern mid-latitudes, from measurements at Mace Head, Ireland. The apparent discrepancy between these published rates of change is resolved if one considers the large interannual variability in the H_2 mixing ratio (see Fig. 1). A good part of that variability is caused by the interannual variability in the H_2 emissions from biomass burning (Langenfelds et al., 2002; see also Section 3.3). In the present case, it is due to the exeptional wild fires in the years 1997–1998 (Langenfelds et al., 2002), which form the end of the observation period of Simmonds et al. (2000) but lie outside that of Novelli et al.

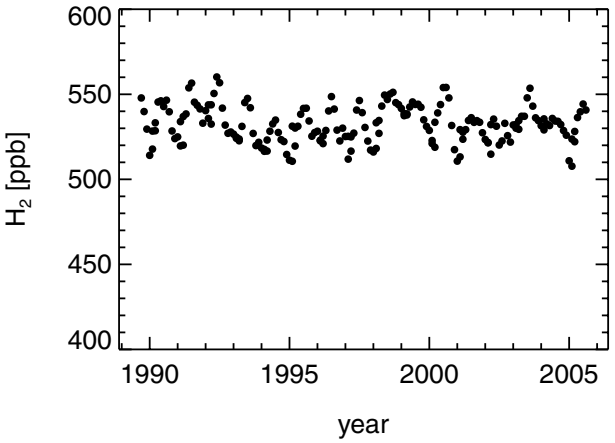

Fig. 1. Mean monthly mixing ratios of H_2 from 1989 to 2005 at Mauna Loa, Hawaii, 20°N latitude. The data are from the Global Monitoring Division (GMD) of NOAA/ESRL (see also Novelli et al., 1999).

(1999). The example also illustrates the danger in deducing a H_2 trend from too short observation periods.

Combined with the earlier data, there is no evidence in the atmospheric concentration measurements for a trend in tropospheric H_2 since 1923 (see Schmidt, 1974; Schmidt and Wetter, 2002). Given the scatter, limited geographical distribution and lack of intercalibration in the early data, this does not preclude a small trend, for instance, of 0.3% yr^{-1} lasting a few decades in the middle of the last century. But it appears to exclude trends of the duration and magnitude observed for tropospheric CH_4 and CO.

The global abundance of CH_4 increased from about 1150 ppb in 1950 to about 1750 ppb in 2000 (Prather et al., 2001), with a rate of increase of about 1% yr^{-1} around 1950 and the decades thereafter, which diminished since the late 1980s to virtually 0 by the year 2000 (Dlugokencky et al., 2003).

The CO increase is less well documented and is established only for the Northern Hemisphere. From historic solar infrared spectra measured at the Jungfraujoch observatory, Switzerland, Zander et al. (1989) derived a mean relative increase in the tropospheric CO column abundance of $(0.85 \pm 0.2)\%$ yr^{-1} between 1950 and 1985. Ice core data from Greenland indicate that the CO increase in the Northern Hemisphere started already in 1860 and averaged a rate of 0.2% yr^{-1} until 1947, the end of the ice core record (Haan et al., 1996). Recent time-series of the CO mixing ratio are available from the CMDL network. Just as those for H_2, they show no long-term change over the last two decades.

Considering that the atmospheric oxidation of CH_4 constitutes the strongest single source of tropospheric H_2—at least today—and that tropospheric H_2 and CO share the same sources, it is rather puzzling that the increases in CO and CH_4 have not been accompanied by a corresponding increase in tropospheric H_2. So far, this question has received little study, and there is no ready answer in the literature.

In contrast to the troposphere, the recent stratosphere exhibits a statistically significant increase in H_2 abundance. From balloon measurements over the period 1988–2000, Rohs et al. (2006) deduced an average increase rate of $(0.3 \pm 0.1)\%$ yr^{-1} for the H_2 mixing ratio between 17 and 30 km altitude—most likely due to the increase in stratospheric CH_4.

2.2. Seasonal variation

The dominant temporal feature in the H_2 mixing ratio of surface air is the seasonal variation. The feature is observed at all stations (Novelli et al., 1999) and shown in more detail by Fig. 2 for a selection of stations covering the latitudes 70°N–80°S (adapted from Price et al., 2007). At most extratropical stations, the seasonal variation is nearly but not quite sinusoidal. The tropical station at Mahe Island indicates a semi-annual pattern. The amplitudes vary with latitude and are smallest at the equator—about 15 ppb peak-to-peak—and increase towards the poles, reaching a peak-to-peak value of 70 ppb (or 15%) at 71°N, and 25 ppb at 88°S, that is, the seasonal variation is much more pronounced in the Northern Hemisphere. In addition, there is good indication that the amplitude in the interior of continents is larger than at coastal stations (see station Ulaan).

The phases also shift systematically with latitude, for example, within the Northern Hemisphere, the maximum is reached in April at high latitudes but in July at low latitudes (see also Hauglustaine and Ehhalt, 2002). Even more interesting is the observation that the phase difference between the two hemispheres is only 3 months instead of the 6 months observed for most other trace gases, a fact that had already been noted by Khalil and Rasmussen (1990). Altogether, the seasonal variations of H_2 exhibit several features not found for other trace gases.

2.3. Latitudinal distribution

The surface stations of the CMDL network also allow to derive the annually averaged latitudinal distribution of the H_2 mixing ratio. This distribution, averaged over the period 1994–2003, is shown in Fig. 3 (adapted from Price et al., 2007; see also Novelli et al., 1999). The annually averaged mixing ratio is the largest at the equator, about 545 ppb, and decreases towards the poles. The decrease is larger in the Northern Hemisphere, reaching 490 ppb at 80°N, compared with only 535 ppb at 88°S. This leads to a significant asymmetry between the hemispheres, the average H_2 mixing ratio in the Northern Hemisphere today being lower by about 3%. From their surface measurements, Novelli et al. (1999) derived an average tropospheric mixing ratio of 531 ± 6 ppb for the years 1991–1996. Since the current trend is negligible, this value should also hold today.

There are indications that the interhemispheric gradient has changed with time. From their measurements between late 1985 and early 1989, Khalil and Rasmussen (1990) deduced a similar but slightly weaker latitudinal gradient, with 517 ppb at Palmer Station, Antarctica, 71.4°S, and 494 ppb at Point Barrow, Alaska, 71.5°N. A much more drastic change is suggested by the earlier measurements of Schmidt (1974, 1978). From his airborne measurements in November 1971 and March 1972 between Frankfurt, Germany, and Rio de Janeiro, Brazil, and a more extended flight campaign in July–August 1974 from Cologne, Germany, 51°N, via Sondrestrom, Greenland, 67°N, to Punta Arenas, Chile, 53°S, and back, Schmidt derived an interhemispheric difference in the upper troposphere, with 1.4% higher H_2 mixing ratios in the Northern Hemisphere. From his data during three ship campaigns, Schmidt derived an even higher interhemispheric difference in surface air, namely 6% in favour of the Northern Hemisphere (Schmidt, 1974, 1978; Schmidt and Wetter, 2002). The H_2 measurements during the campaigns were made over the North Atlantic between about 40°N and 50°N latitude in June 1971 (Meteor cruise #23-III), over the North Atlantic between about 20°N and 50° N in October 1973 (Meteor cruise #32-I)

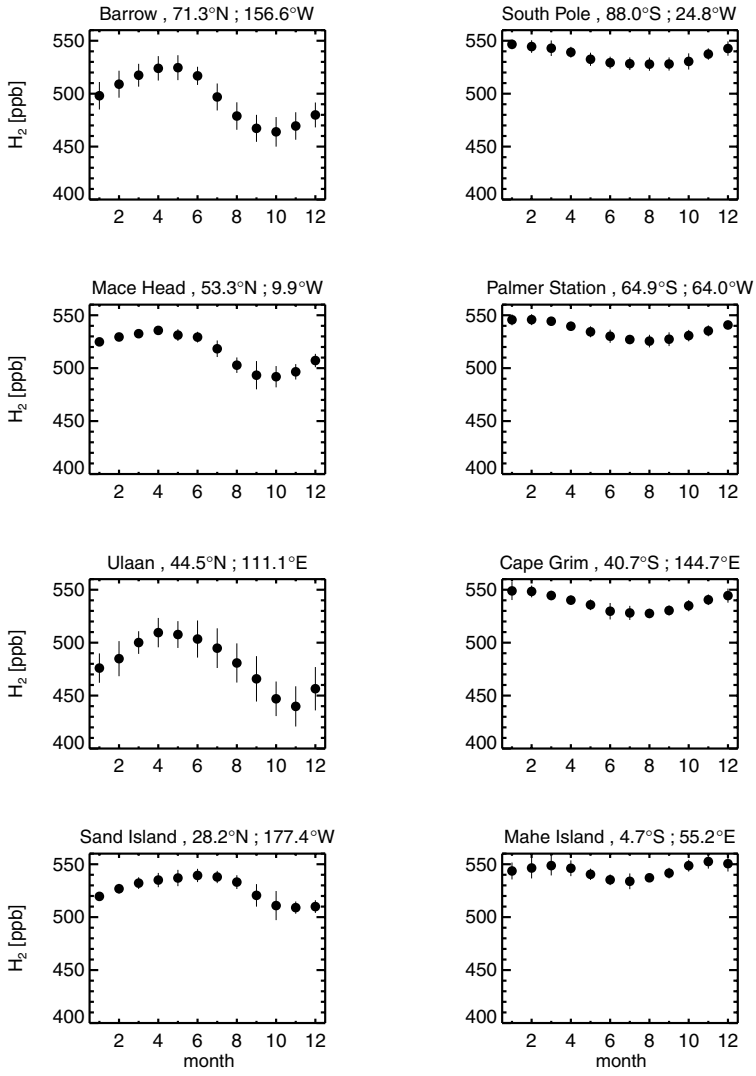

Fig. 2. Average seasonal variation of the H_2 mixing ratio at eight CMDL network sites between 1994 and 2003. Error bars represent the standard deviations (Adapted from fig. 7, Price et al., 2007; the data are from GMD, NOAA/ESRL).

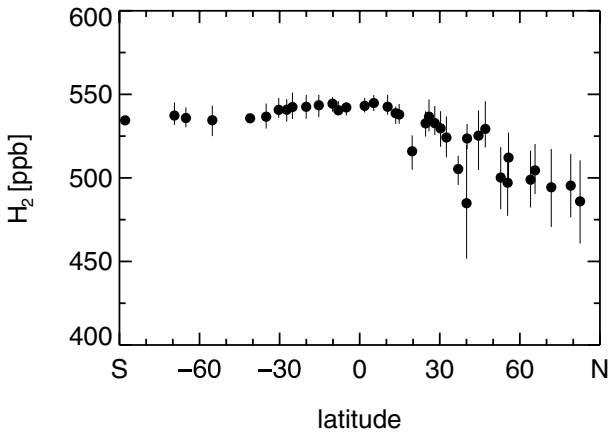

Fig. 3. Average latitudinal distribution of the H_2 mixing ratio between 1994 and 2003 derived from the CMDL surface network sites. Error bars represent the standard deviations (Adapted from fig. 6, Price et al., 2007; the data are from GMD, NOAA/ESRL).

and over the North and South Atlantic between about 20°N and 60°S in November–December 1971 (aboard the R.R.S. Shackleton). Obviously, only one campaign covered both hemispheres. Averaging the data from all three campaigns could thus result in a substantial bias in the derived interhemispheric difference, since the average H_2 mixing ratio for the Northern Hemisphere includes data from an extra year and extra season, and since the H_2 mixing ratio in a hemisphere shows considerable interannual variability and seasonal variation (see Figs. 1 and 2). We, therefore, regard the historic interhemispheric difference of 6% for surface air as less reliable than that for the upper troposphere of 1.4%. The value for the upper troposphere does not quite constitute an annual average, but it includes the data from three seasons and all seem to indicate that the interhemispheric gradient in the early 1970s was reversed from that today. The transition, which appears to have taken place in the late 1970s to early 1980s, points to a shift in the hemispheric balance of sinks and sources. This effect cannot be explained by an

increased production of H_2 from the oxidation of CH_4, which must have impacted both hemispheres equally. It requires additional changes. One explanation, which could solve the question of both the reversal and the missing trend, would be an increase in soil uptake possibly owing to climate or land use change. So far, the question of a possible trend reversal has attracted little attention, and the literature offers no explanation.

2.4. Vertical distribution

There are a number of early studies that attempted to characterize the vertical distribution of H_2 in the troposphere; Schmidt (1978) obtained around 60 vertical profiles during landing and take off in the course of his flight campaign 1974. These profiles extended from the surface to about 12 km altitude and were averaged in six latitude bands between 60°S and 70°N to look for a latitudinal dependence in the vertical profiles (Schmidt, 1978). Ehhalt et al. (1977) collected monthly samples above Scotts Bluff, Nebraska, 42°N, and the Pacific Ocean about 34°N, 125°W, 200 km west of San Luis Obispo, CA, to investigate the possibility of a seasonal dependence in vertical H_2 profiles. In addition, there are vertical profiles from various other locations in Europe and North America (Ehhalt et al., 1977; Seiler et al., 1978; Fabian et al., 1979). The individual profiles often showed substantial variations vertically and among each other. Their salient average features can be summarized as follows:

The vertical distribution of H_2 in the free troposphere was on average rather uniform. No significant vertical gradients were observed except for the average profile in the latitude band from 50°N to 70°N, where Schmidt (1978) found a substantial increase throughout the troposphere in July and August, reaching from about 480 ppb at the surface to about 550 ppb at the tropopause (10 km). Since most of the individual profiles contained in this average came from rural Canada, he assigned this gradient to the uptake of H_2 at the earth's surface.

Given the scatter in the individual profiles, the search for a seasonal change in the vertical pattern of H_2 in the free troposphere proved inconclusive, although temporal variations of the order of about 10% on the timescale of a year could not be excluded (Ehhalt et al., 1977).

On the other hand, the data from the planetary boundary layer (about 1 km in height) did exhibit significant gradients at some locations. The measurements over the Pacific at San Luis Obispo, for instance, showed a strong increase of the H_2 mixing ratio towards the ocean surface in all seasons (Ehhalt et al., 1977). The origin of the local H_2, however, remained unexplained.

In Fig. 4 (adapted from Price et al., 2007), we present examples of recent vertical profiles of the H_2 mixing ratio from the GMD programme, namely, seasonally averaged profiles over Poker Flat, Alaska, 65°N (2002–2004); Park Falls, Wisconsin 45.9°N (2002–2004), and Cook Islands, 21.4°S, 160.4°W (2003–2004). Here, the vertical profiles over the continental sites exhibit a clear increase throughout the observed altitude range (up to 7 km)—confirming the earlier observations by Schmidt (1978). The gradient is present in all seasons but maximizes in the fall. As a consequence, the pattern of the vertical H_2 profile varies slightly but systematically with the season.

In contrast, the maritime profiles in the Southern Hemisphere exhibit much more uniform H_2 mixing ratios between the surface and 6 km, the maximum altitude sampled, and vary little with season.

There is also a substantial set of monthly vertical H_2 profiles over Cape Grim, Tasmania, measured by the CSIRO. The profiles range from about 150 m to about 8000 m altitude and cover the period from August 1991 to September 2000. The data are available from Ray.Langenfelds@CSIRO.AU. The earlier profiles from April 1992 to February 1997 have been summarized by Pak (2000). They exhibit a seasonal variation at all altitudes of about the same amplitude but a forward phase shift of about 2 months in the upper troposphere. This results in a regular change in the vertical H_2 gradient from decrease with altitude in the second quarter to an increase in the fourth quarter of the year.

In summary, although the globally averaged vertical profile of H_2 may be rather uniform, there are regions with strong vertical gradients of up to 10% across the vertical extent of the troposphere. They have been observed over extended regions with large surface losses but should also be present—with inverse sign—over regions with high surface sources, that is, heavily populated and industrialized areas. These gradients can change with season.

2.5. Tropospheric burden of H_2

From their average tropospheric mixing ratio of $\bar{X} = 531 \pm 6$ ppb, Novelli et al. (1999) calculated a tropospheric burden (B) of 155 ± 10 Tg H_2. Without being explicitely stated, B was apparently calculated from $B = (\bar{X} m_{H_2}/m_{air}) 0.82 \times M_{At}$ where $M_{At} = 5.14 \times 10^{21}$ g is the total mass of the atmosphere (Trenberth and Guillemot, 1994) and 0.82 is the fraction of air residing in the troposphere. $m_{H_2}/m_{air} = 2/29$ is the molecular mass ratio of H_2 and air. Since it is based on measurements, we will adopt their estimate here. We note, however, that the estimates of the tropospheric burden by other authors vary between 136 and 159 Tg H_2 (see Table 1, below), which is somewhat surprising, given the fact that tropospheric H_2 is rather uniformly distributed and that the average mixing ratios—where given—do not differ by more than 10 ppb from the 531 ppb obtained by Novelli et al. (1999), for example, Hauglustaine and Ehhalt (2002): 540 ppb; Price et al. (2007): 521 ppb. None of the authors listed in Table 1 gave sufficient details to repeat his estimation. However, we tentatively suggest that the values of the tropospheric air mass used by these authors must have differed up to 5% from that used by Novelli et al. (1999). The average over

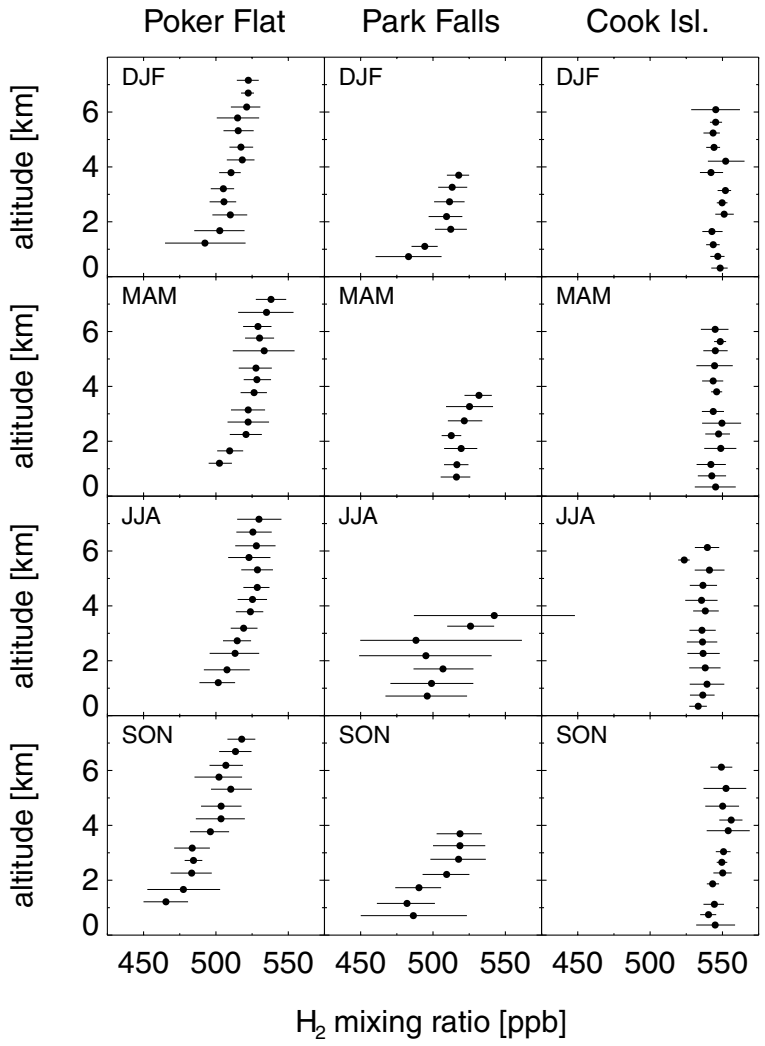

Fig. 4. Seasonally averaged vertical profiles of the H_2 mixing ratio over Poker Flat, 65.1°N, 147.3°W (2002–2004); Park Falls, 45.9°N, 90.3°W, (2002–2004) and Cook Island, 21.4°N, 160.4°E (2003–2004). Error bars represent the standard deviation (Adapted from fig. 8, Price et al., 2007; the data are from GMD, NOAA/ESRL).

the tropospheric burdens listed in Table 1 is 148 Tg H_2 (excluding our own) and its standard deviation is ±8 Tg H_2, in good agreement with the value of 155 ± 10 Tg from Novelli et al. (1999).

2.6. *Stratospheric distribution of H_2*

The early studies also provided information on the vertical distribution of the H_2 mixing ratio in the stratosphere (Ehhalt et al., 1977; Ehhalt and Tönnißen, 1979; Fabian et al., 1979). Just as in the troposphere, the average vertical distribution in the lower and middle stratosphere proved to be relatively uniform. Figure 5 (adapted from Ehhalt et al., 1977) presents the average vertical profile of stratospheric H_2 around 30° latitude in the 1970s. It is based on the results of six balloon flights, mostly over Palestine, TX, 32°N, and extended to 50 km altitude with the help of two rocket samples collected over White Sands Missile Range, NM, 31°N (Scholz et al., 1970; Ehhalt et al., 1975). It reveals a slight increase from 520 ppb at the tropopause to a maximum of about 550 ppb at 30 km and a decrease in the upper stratosphere to 400 ppb at the stratopause. Stratospheric profiles at 44°N over Europe (Fabian et al., 1979) and at 52°N over North America (Heidt et al., 1979) rather indicated a slight decrease between tropopause and 35 km altitude, suggesting the possibility of a slight latitudinal gradient in the lower stratosphere of the 1970s (Ehhalt and Tönnißen, 1979).

There are a number of recent balloon or aircraft borne measurements of stratospheric H_2, notably by the Institute of Meteorology and Geophysics of the University of Frankfurt, Germany (see Engel et al., 2005; Rohs et al., 2006), and by CMDL (cf. Hurst et al., 1999). Unfortunately, most of these data have not yet been published in the open literature. Some of the results, however, can be gleaned from papers utilizing part of the data. From samples collected on a balloon launched on 20 September 1993, in Aire sur l'Adour, France, 43.7°N, Zöger et al. (1999) measured a vertical profile, which indicates

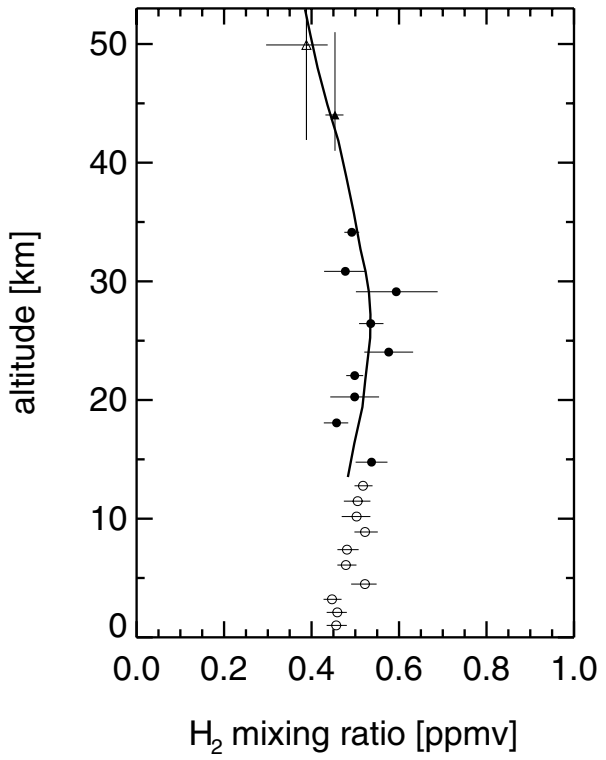

Fig. 5. Average vertical profile of the H_2 mixing ratio in the stratosphere at 30° latitude in the 1970s (Adapted from Ehhalt et al., 1977). Full circles: Average over the measurements from 6 balloon flights between 1972 and 1975—most at Palestine, TX, 32°N; one over Parana, Argentina, 30°S. Open circles: Average tropospheric profile at the time, from aircraft flights. Open triangle: Result from a rocket flight on 24 September 1968. Full triangle: Result from a rocket flight on 23 May 1973. The vertical bars indicate the height interval of the rocket sampling. The error bars indicate the standard error of the measurement in the case of the rocket samples and the standard deviation of the mean in the case of balloon and aircraft samples. The heavy line is a hand drawn average through the stratospheric data.

an increase from 545 ppb near the tropopause to 560 ppb around 32 km altitude, albeit with a large uncertainty. A similar result was obtained by Hurst et al. (1999), who measured H_2 and CH_4 aboard the NASA ER-2 aircraft from May 1995 to December 1996 and between 3°S and 60°N during the Stratospheric Tracers of Atmospheric Transport (STRAT) campaign. They found a slight anticorrelation between the H_2 and CH_4 mixing ratios, resulting in a linear slope of -0.027 ± 0.003 ppbH_2/ppbCH_4. Since CH_4 decreases monotonically with altitude in the stratosphere, this corresponds to an increase of H_2 with height. For an average CH_4 profile at mid-latitudes, this slope translates into a gradient of about 1.3 ppbH_2/km in the lower stratosphere to about 22 km altitude. A vertical profile measured by Röckmann et al. (2003) from balloon samples collected over Aire sur l'Adour in October 2002 and another deduced from the measurements aboard the NASA ER-2 in January–March 2000 between 65°N–80°N and 13°E–63°E by Rahn et al. (2003) show too much variability to deduce as small a gradient as those mentioned above and would have to be considered uniform. Finally, in a brief summary, Engel et al. (2005) present the H_2 mixing ratios measured during the European polar stratospheric cloud and Lee wave experiment (EUPLEX) in winter 2003 over northern Europe against N_2O as vertical coordinate. When transformed to geometric height, using a mid-latitude N_2O profile, these data show an increase in the H_2 mixing ratio from about 540 ppb at the tropopause to about 560 ppb at 30 km altitude and a decrease above, that is, a profile of the form shown in Fig. 5 for 30°N in the 1970s. As a first approximation, we therefore assume that the current vertical profile of the H_2 mixing ratio at northern mid-latitudes has a form similar to that in Fig. 5.

Owing to the lack of published observations, the seasonal and spatial distributions of the H_2 mixing ratio in the stratosphere are not well characterized. On the other hand, it appears that the seasonal and spatial distributions of H_2 in the current troposphere are fairly well covered by observations. Their various features can be well understood in terms of the distributions of sources and sinks of H_2, and they have been simulated reasonably well by recent 3-D models (Hauglustaine and Ehhalt, 2002; Sanderson et al., 2003, Price et al., 2007). This will be discussed in the final section.

3. Sources of atmospheric H_2

The atmospheric burden of H_2 is maintained by a variety of sources. These can be broadly categorized into surface sources, such as fossil fuel combustion or biomass burning, and volume sources caused by the photochemical degradation of organic compounds, such as CH_4 or isoprene (C_5H_8) within the troposphere itself. Both categories introduce about equal amounts of H_2. The major sources and the source strengths published by various authors in the past decade are summarized in Table 1. For completeness, Table 1 also contains the other budget terms: burden, sinks, and lifetime. Information on earlier budgets is found in Warneck (1988). Not all of the entries in Table 1 are independent estimates. Some are taken over from previous budgets; others are different adaptations of the same data sets. Where important, this will be pointed out in the following discussion of the individual sources. To illustrate the methods of estimation and their errors, we will derive estimates for each of the sources listed in Table 1.

3.1. Photochemical oxidation of CH_4

CH_4 is the longest lived and most abundant organic molecule in the atmosphere. Its degradation, which provides the largest single source of tropospheric H_2, is initiated by the reaction with OH:

$$CH_4 + OH \rightarrow CH_3 + H_2O. \qquad \text{(R1)}$$

Table 1. Major global tropospheric sources and sinks of H_2 (Tg H_2 yr^{-1}) from various authors

	Novelli et al. (1999)	Hauglustaine and Ehhalt (2002)	Sanderson et al. (2003)	Rhee et al. (2006a)	Price et al. (2007)	Xiao et al. (2007)	This work
Fossil fuel	15 ± 10	16	20.0	15 ± 6	18.3	15 ± 10	11 ± 4
Biomass burning	16 ± 5	13	20.0	16 ± 3	10.1	13 ± 3	15 ± 6
Biofuel					4.4		
N_2 fixation, ocean	3 ± 2	5	4.0	6 ± 5	6.0		6 ± 3
N_2 fixation, land	3 ± 1	5	4.0	6 ± 5	0		3 ± 2
Photochemical production							
from methane	26 ± 9		15.2		24.5		23 ± 8
from VOC	14 ± 7		15.0		9.8		18 ± 7
total	40	31	30.2	64 ± 12	34.3	77 ± 10	41 ± 11
Sources total	77 ± 16	70	78.2	107 ± 15	73	105 ± 10	76 ± 14
Oxidation by OH	19 ± 5	15	17.1	19 ± 3	18	18 ± 3	19 ± 5
Soil uptake	56 ± 41	55	58.3	88 ± 11	55 ± 8.3	85 ± 5	60^{+30}_{-20}
Sinks total	75 ± 41	70	75.4	107 ± 11	73	105[a]	79^{+30}_{-20}
Tropospheric Burden, Tg H_2	155 ± 10	136	172[b]	150[c]	141	149 ± 23	$155^{d} \pm 10$
Tropospheric Lifetime, yr	2.1	1.9	2.2[b]	1.4	1.9	1.4	2.0

[a]Includes export to stratosphere of 1.9 Tg H_2 yr^{-1}.
[b]Model domain reached 100 hPa; thus the burden includes about 1/2 of the stratosphere. Reduced to a troposphere holding 0.82 of the total air mass the burden would be 157 Tg H_2 and the tropospheric lifetime 2.0 yr.
[c]Calculated from sources and lifetime.
[d]From Novelli et al. (1999).

The rate constant is $K_1 = 2.45 \times 10^{-12} \times \exp(-1775/T)$ molecule^{-1} cm^3 s^{-1} (Sander et al., 2006). Reaction (R1) is also the rate limiting step in the ensuing chain of reactions that eventually leads to the formation of formaldehyde (HCHO), with a yield of virtually 1 under tropospheric conditions. The complete reaction scheme is discussed in Novelli et al. (1999). HCHO is decomposed by three reactions

$$\mathrm{HCHO + OH \rightarrow HCO + H_2O}, \quad \text{(R2)}$$

$$\mathrm{HCHO + h\nu \rightarrow HCO + H}, \quad \text{(R3a)}$$

$$\mathrm{HCHO + h\nu \rightarrow H_2 + CO}. \quad \text{(R3b)}$$

In addition a small fraction, about 5%, of HCHO is removed by rainout and dry deposition at the earth's surface.

The formyl radical (HCO) generated in reactions (R2) and (R3a) rapidly reacts via

$$\mathrm{HCO + O_2 \rightarrow CO + HO_2}. \quad \text{(R4)}$$

Thus, 95% of the HCHO (and consequently of the CH_4) eventually produce CO, but only a much smaller fraction defined by reaction (R3b) generates H_2. That fraction (F_{H_2}) is given by the product $0.95 \times F \times \phi_{3b}$, where F is the fraction of HCHO reacting by photolysis and ϕ_{3b} the yield of the molecular photolysis channel (R3b). Novelli et al. (1999) have estimated the globally averaged values of these parameters to $F = 0.65 \pm 0.15$ and $\phi_{3b} = 0.6 \pm 0.1$. The F_{H_2} averaged over the troposphere is thus calculated to $\overline{F_{H_2}} = 0.37$.

According to this reaction scheme the local production rate of H_2 from the oxidation of CH_4 is given by

$$P_{CH_4,H_2} = K_1(T) \times [OH] \times [CH_4] \times F_{H_2}, \quad (1)$$

where the brackets denote the local number density in units of molecule cm^{-3}.

The global, annual production rate, $\overline{P_{CH_4,H_2}}$, is obtained by integration of this product over time and space, which 2-D and 3-D models can perform from internally generated fields of [OH], [CH_4] and $K_1(T)$. Novelli et al. (1999), as well as the authors of earlier estimates, had to approximate the average of the product by a product of properly weighted averages:

$$\overline{P_{CH_4,H_2}} = \bar{F}_{H_4} K_1(\bar{T}) \overline{[OH]} \int [CH_4] dV. \quad (2)$$

Here $\int [CH_4] dV$ represents the tropospheric burden of CH_4, $\overline{[OH]}$ is an empirical global and annual average of the tropospheric OH concentration and $\overline{T}$ an effective average temperature. The last three terms in eq. (2) define the tropospheric loss rate of CH_4 due to reaction with OH:

$$\bar{L}_{CH_4,OH} = K_1(\overline{T}) \times \overline{[OH]} \times \int [CH_4] dV. \quad (3)$$

As Prather and Spivakovsky (1990) demonstrated, expression (3) is a quite good approximation for the tropospheric loss of any trace gas that is uniformly or nearly uniformly distributed, which is the case for CH_4. To be compatible, $\overline{[OH]}$ and $\overline{T}$ should be calculated with the same averaging procedure. The empirical $\overline{[OH]}$ is generally derived from the global budget of methyl chloroform (CH_3CCl_3), an anthropogenic trace gas with well-defined source strength and an atmospheric lifetime of about 5 yr (Prinn et al., 1995). Various approaches, 2-D and 3-D models, were employed to determine $\overline{[OH]}$. The more recent literature lists tropospheric $\overline{[OH]}$ as $(11 \pm 2) \times 10^5$ cm^{-3} (Montzka et al., 2000), 11.6×10^5 cm^{-3} (Spivakovsky et al., 2000), 10×10^5 cm^{-3} (Krol and Lelieveld, 2003), $(9.8 \pm 0.9) \times 10^5$ cm^{-3} (averaged from 1980 to 2000, Bousquet et al., 2005) and $(10.9^{+0.8}_{-0.9}) \times 10^5$ cm^{-3} (averaged from 1978 to 2004, Prinn et al., 2005). The average over these numbers is 10.7×10^5 cm^{-3}.

These studies also showed that $\overline{[OH]}$ varied on a decadal scale.

From eq. (2), Novelli et al. (1999) estimated $\overline{P_{CH_4,H_2}}$ to 26 ± 9 Tg H_2 yr^{-1}, using a tropospheric CH_4 burden for 1992 of (4000 ± 400) Tg CH_4, a $\overline{[OH]} = (9.7 \pm 0.6) \times 10^5$ cm^{-3}, (Prinn et al., 1995), a $K_1(277) = (4.0 \pm 0.2) \times 10^{-15}$ molecule^{-1} cm^3 s^{-1} and the $\overline{F_{H_2}}$ indicated above. Actually, the straightforward product of these numbers would yield an $\overline{P_{CH_4,H_2}} = 22.6$ Tg H_2 yr^{-1}. For their estimate of 26 Tg yr^{-1}, Novelli et al. (1999) calculated an upper bound by assuming all errors to be positive, a corresponding lower bound and averaged over the two.

To update this estimate, we will use the average $\overline{[OH]} = 10.7 \times 10^5$ cm^{-3} from above, an updated $\overline{T} = 272$ K (Spivakovsky et al., 2000) with a corresponding $K_1(272) = 3.59 \times 10^{-15}$ molecule^{-1} cm^3 s^{-1}, and $\overline{F_{H_2}} = 0.37$. We further use a tropospheric burden of 4140 Tg CH_4. It is based on the value of 4000 Tg CH_4 from Novelli et al. (1999) and adjusted to 2005 by multiplication with the ratio of the average tropospheric CH_4 mixing ratio in 2005 (IPCC, 2008) to that in 1992 (IPCC, 1995): 1774/1714. This gives $\overline{P_{CH_4,H_2}} = (23.2 \pm 8)$ Tg H_2 yr^{-1} from the direct product of eq. (2). The error assigned assumes the same relative error as estimated by Novelli et al. (1999).

This value agrees well with the latest estimate of $\overline{P_{CH_4,H_2}} = 24.5$ Tg yr^{-1} by a 3-D model (see Price et al., 2007, in Table 1). But it is barely within the error bounds of the only other published 3-D estimate of 15.2 Tg yr^{-1} by Sanderson et al. (2003). The reason for the difference is not clear, except that it is not likely due to the OH field, since that model also correctly reproduces the empirically deduced lifetime of CH_3CCl_3. We will adopt 23 ± 8 Tg yr^{-1} as the current best estimate for the tropospheric production of H_2 from CH_4.

Since [OH] (Spivakovsky et al., 2000) and $K_1(T)$ maximize in the tropics and in the summer hemisphere, the H_2 production from CH_4 shows strong latitudinal and seasonal variations, with maxima about the equator and in summer.

3.2. Photochemical oxidation of VOC

Besides CH_4, there are a number of other organic molecules whose atmospheric oxidation leads to the production of H_2. We summarize these under the term volatile organic compounds (VOC). The most important of these are isoprene, the monoterpenes ($C_{10}H_X$) and methanol (CH_3OH), which are released in large quantities by land vegetation. Like CH_4, all the VOC are attacked by OH and eventually form HCHO, the immediate precursor of H_2 through reaction (R3b). The estimate of their global production rates is, however, hampered by three factors:

(1) The VOC are much more reactive than CH_4. Isoprene and the monoterpenes, for instance, are oxidized within hours after their emission. As a consequence, their distributions are highly non-uniform and not well known. To estimate their contribution to the H_2 budget, one has to rely on their respective global emission rates, which are much more uncertain than the global burden of CH_4.

(2) Their chemistry is often more complex and less well established than that of CH_4. In particular, the yield of HCHO per carbon atom in the oxidation of VOC is substantially less than 1 and depends on the local chemical environment, notably the NO_X concentration (Palmer et al. 2006; cf. Hatakeyama et al., 1991; Miyoshi et al., 1994). Thus, the yield of HCHO from VOC is much more variable and uncertain than that from CH_4.

(3) Finally, there are some other reaction paths of VOC that form H_2, such as ozonolysis of the alkenes or the photolysis of glyoxal, which is formed in the oxidation of C_5H_8. These contribute less than 10% but need to be considered.

At first sight, the estimates for the photochemical production of H_2 in Table 1 appear to reflect the large uncertainties just mentioned—not so much in the quoted errors but in the range of values, which brackets 30–77 Tg yr^{-1} for the total photochemical production from CH_4 and VOC. A second look, however, tells us that the two high estimates 64 ± 12 Tg yr^{-1} (Rhee et al., 2006a) and 77 ± 10 Tg yr^{-1} (Xiao et al., 2007) result from a different approach than the others. They are top down calculations, which used inverse modelling (Xiao et al., 2007) or the seasonal variation in the deuterium content of H_2 (Rhee et al., 2006a) to deduce the global sink strengths of the soil uptake along with the photochemical production rate from VOC (see Section 4.2.2 for details). The other estimates in Table 1 are bottom up. They prescribe the global distribution and strengths of the precursor emissions based on literature values and calculate the resulting H_2 production through 3-D chemical transport models (Hauglustaine and Ehhalt, 2002; Sanderson et al., 2003; Price et al., 2007) or approximatively through the use of globally averaged yields (Novelli et al., 1999). For these the estimated global H_2 production from VOC ranges from 30 to 40 Tg yr^{-1} of which, more than one-half come from the oxidation of CH_4.

To resolve the discrepancy between bottom up and top down estimates and to obtain a better grasp of the errors involved, we will update the estimates for the H_2 production from C_5H_8, monoterpenes and CH_3OH. According to Novelli et al. (1999), the global production rate of H_2 from the oxidation of a given VOC_i can be approximated by

$$\overline{P_{\mathrm{VOC_i,H_2}}} = S_i \times \overline{Y_i} \times \overline{F'_{\mathrm{H_2}}} \times (m_{\mathrm{H_2}}/m_{\mathrm{c}}). \quad (4)$$

Here S_i is the global emission rate of VOC_i in Tg C yr^{-1}, $\bar{Y}_i$ is the globally averaged yield of HCHO per carbon atom in VOC_i and $\overline{F'_{\mathrm{H_2}}}$ is the average fraction of HCHO that forms H_2. The mass ratio $m_{\mathrm{H_2}}/m_{\mathrm{c}} = 2/12$ converts to Tg H_2. $\overline{F'_{\mathrm{H_2}}}$ is analogous to $\overline{F_{\mathrm{H_2}}}$ for CH_4 (Section 3.1) and consists of the same three factors: a factor of 0.95 to account for the dry deposition of HCHO, a factor $F = 0.65 \pm 0.15$ for the fraction of HCHO that undergoes photolysis and a factor $\overline{\Phi'_{3b}}$ for the yield of the molecular photolysis channel (reaction R3b). $\overline{\Phi'_{3b}} = 0.5 \pm 0.1$, that is, a little lower than ϕ_{3b} for CH_4, to account for the fact that the HCHO generated from C_5H_8 or the monoterpenes resides closeer to the earth's surface because of their short life times (Novelli et al., 1999). The two other factors are numerically identical to those for CH_4. We note that for the short lived VOC, the fraction of HCHO dry deposited might well be higher than suggested by Novelli et al., 1999, because it is generated much closer to the ground. In addition the presence of high levels of reactive VOC might reduce the concentration of OH, allowing a larger fraction of HCHO to photolyse. Since both effects cancel to a certain degree and to remain consistent with the estimates of Novelli et al. (1999), we retain their value of 0.31 for $\overline{F'_{\mathrm{H_2}}}$.

Past estimates of the global C_5H_8 emissions range from 175 to 750 Tg C yr^{-1} (see Steiner and Goldstein, 2007, for an overview). The most recent estimate by Guenther et al. (2006) gives a range of 440–660 Tg C yr^{-1}. To accommodate the larger range in the past and to acknowledge the fact that the more recent values cluster around 500 Tg C yr^{-1}, we adopt a global emission of C_5H_8, $S_{is} = 500 \pm 250$ Tg C yr^{-1}.

Since the detailed photochemical breakdown of C_5H_8 is complex and not completely understood, the different reaction mechanisms in use give somewhat different yields of HCHO, Y_{is}. Palmer et al. (2006) in their model calculations of HCHO from C_5H_8 found $Y_{is} = 0.5$ HCHO/C for 1 ppb NO_X and 0.47 HCHO/C for 0.1 ppb NO_X after a 5-day-reaction period, when using the Master Chemical Mechanism version 3.1 (Saunders et al., 2003). The corresponding Y_{is} for their own GEOS-CHEM chemical mechanism were $Y_{is} = 0.43$ HCHO/C for 1 ppb NO_X and 0.29 HCHO/C for 0.1 ppb NO_X. The calculations also indicated that the main effect of low NO_X levels is a slow down of the formation of HCHO. Given enough time, the eventual HCHO yields for low (0.1 ppb) and high (1ppb) NO_X were not as different as assumed in the past. Palmer et al. (2006) also noted that at an experimental site (PROPHET) measured HCHO concentrations, and C_5H_8 fluxes suggested a 30% lower Y_{is} than their own mechanism. A lower empirical yield was also found by Millet et al. (2006), who estimated an average $Y_{is} = 0.32 \pm 0.1$ over North America from the correlation of HCHO and C_5H_8 columns measured from aircraft during the INTEX-A campaign. Altogether, current information still admits a range in Y_{is} of 0.2–0.5. This is not much improvement over the range of 0.2–0.6, which Novelli et al. (1999) had assumed based on the then available information. Based on the new range, we adopt a central value and error for $\overline{Y_{is}}$ of 0.35 ± 0.15.

With the new figures for S_{is} and $\overline{Y_{is}}$ and $\overline{F'_{H_2}}$ from above, we obtain a global H_2 production rate from C_5H_8 oxidation of $\overline{P_{is,\mathrm{H_2}}} = 9 \pm 6$ Tg H_2 yr^{-1}. It includes both oxidation initiated by OH (∼90%) and by O_3 (∼10%).

The error in $\overline{P_{is,\mathrm{H_2}}}$ is obtained from the propagation of the errors given above for the individual factors. It is somewhat ill-defined. Since we used the full range of the (few) available estimates of S_{is} and $\overline{Y_{is}}$ to define their error, and since these are the largest sources of uncertainty, the error given for $\overline{P_{is,\mathrm{H_2}}}$ and for $\overline{P_{mo,\mathrm{H_2}}}$ and $\overline{P_{\mathrm{CH_3OH,H_2}}}$ below probably exceeds 1σ bounds somewhat. Nevertheless, to be conservative, we will adopt them here as 1σ errors.

A similar estimate can be made for the monoterpenes. The more recent values for the total emission rates for these species fall in a surprisingly narrow range: 127–147 Tg C yr^{-1} (see Steiner and Goldstein, 2007, and references therein). For our calculation we adopt $S_{mo} = 140 \pm 20$ Tg C yr^{-1}. Monoterpene oxidation is initiated about equally by OH and O_3. The HCHO yields, Y_{mo}, are lower than that for C_5H_8. Novelli et al. (1999) assumed $\overline{Y_{mo}} = 1/2\overline{Y_{is}}$. Palmer et al. (2006), using the Master Chemical Mechanism, calculated total HCHO yields for a 5-day-reaction period of $Y_{mo,\alpha} = 0.31$ HCHO/C for $NO_X =$ 1 ppb and 0.24 HCHO/C for $NO_X = 0.1$ ppb in the oxidation of α-pinene and a $Y_{mo,\beta}$ of 0.27 and 0.18, respectively, for β-pinene. A $\overline{Y_{mo}} = 0.2 \pm 0.1$ HCHO/C covers both ranges and will be adopted here for the average yield. With these figures for S_{mo}, and $\overline{Y_{mo}}$ and the $\overline{F'_{\mathrm{H_2}}}$ from above, we calculate a global production rate of H_2 from the oxidation of monoterpenes of $\overline{P_{mo}} = 1.4 \pm 0.8$ Tg H_2 yr^{-1}.

Methanol is another VOC released copiously by land plants. Including other more minor sources, such as biomass burning, its total surface emissions range from 20 to 140 Tg C yr^{-1} (Galbally and Kirstine, 2002; Heikes et al., 2002; Tie et al., 2003; Singh et al., 2004; Steiner and Goldstein, 2007). Weighing the various ranges given by these authors suggests a mid value and bounds of $S_{\mathrm{CH_3OH}} = 70 \pm 50$ Tg C yr^{-1} for the total surface emissions, which will be adopted here. This estimate excludes CH_3OH generated from the photo-oxidation of other VOC within the atmosphere to avoid double counting. In the atmosphere, CH_3OH reacts with OH on a timescale of about 3 weeks and eventually forms HCHO. But unlike CH_4, CH_3OH is soluble, and its

Table 2. H_2 Production from biogenic VOC

	Novelli et al. (1999)		Sanderson et al. (2003)		Price at al. (2007)		This work	
Species(	Precursor emissions (Tg C yr^{-1})	H_2 production (Tg H_2 yr^{-1})	Precursor emissions (Tg C yr^{-1})	H_2 production (Tg H_2 yr^{-1})	Precursor emissions (Tg C yr^{-1})	H_2 production (Tg H_2 yr^{-1})	Precursor emissions (Tg C yr^{-1})	H_2 production (Tg H_2 yr^{-1})
Isoprene	200–500	2–7 (4.5)	446[a]	11	397[b]	5.6	500 ± 250	9 ± 6
Methanol	included in other VOC			0.3	43[b]	2.0	70 ± 50	2.2 ± 1.8
Monoterpenes	100–200	0.2–5 (2.6)	not considered		150[b]	1.5	140 ± 20	1.4 ± 0.8
Acetone	included in other VOC			0.5	16[b]	0.7		0.6[c]
Sum of other VOC	100–400	0.4–12 (6.2)	44[a]	1.0[d]	not considered		250 ± 150	2.6 ± 2.1

[a]from Collins et al. (1997).
[b]from Duncan et al. (2007).
[c]average of estimates by Sanderson et al. (2003), and Price et al. (2007).
[d]estimated from a) and Table II Sanderson et al. (2003).

removal by rainout and dry deposition is much more important than that for CH_4. As a consequence, its HCHO yield is significantly less than 1. From the sink strengths listed in Galbally and Kirstine (2002), Heikes et al. (2002) and Tie et al. (2003), one can estimate the fraction of CH_3OH reacting with OH. It varies from 0.37 (Heikes et al., 2002) to 0.73 (Galbally and Kirstine, 2002), depending on whether the oceans are considered as a sink or as a temporary reservoir. To accommodate both views, we choose a mid-value and error bounds of $\overline{Y_{CH_3OH}} = 0.5 \pm 0.2$ for the HCHO yield from CH_3OH oxidation. With these values and $\overline{F_{H_2}}$ for CH_4 (Section 3.1), eq. (4) gives a H_2 production from CH_3OH of $\overline{P_{CH_3OH,H_2}} = 2.2 \pm 1.8$ Tg H_2 yr^{-1}.

The present H_2 production rates—$\overline{P_{is,H_2}}$, $\overline{P_{mo,H_2}}$ and $\overline{P_{CH_3OH,H_2}}$—are listed in Table 2 together with their precursor emissions and compared with earlier estimates from the literature. The present values fall well within the ranges spanned by the previous estimates. For acetone, which is not calculated here, we adopt a H_2 production rate of 0.6 Tg H_2 yr^{-1}, the average of the estimates by Sanderson et al. (2003) and Price et al. (2007).

There are other biogenic emissions of alkanes, alkenes, alcohols, aldehydes, etc., total of which—including CH_3OH—has been estimated to about 500 Tg C yr^{-1} (Guenther et al., 1995). Its error range is large (see Koppmann, 2007). Excluding CH_3OH and acetone, whose emissions are specified in Table 2, we will assume a source strength for these emissions of $S_o = 250 \pm 150$ TgC yr^{-1}. Novelli et al. (1999) assumed an average HCHO yield from the photo-oxidation of these species of $\bar{Y}_o = 0.2 \pm 0.1$, which we also adopt here. With these values and $\overline{F'_{H_2}}$ from above, eq. (4) gives a H_2 production $\overline{P_{o,H_2}} = 2.6 \pm 2.1$ Tg H_2 yr^{-1}.

Table 3. H_2 Production from the photo-oxidation of VOC from biomass burning and fossil fuel use (after Sanderson et al., 2003)

Species	Globally annually integrated H_2 source strength (Tg H_2 yr^{-1})
Ethane	0.2
Propane	0.3
Butane	1.2
Ethene	0.8
Propene	0.6
Formaldehyde[a]	0.1
Acetaldehyde[a]	0.1
Sum	3.3

[a]From direct emission only.

Finally, a variety of VOC is also emitted by biomass burning and the use of fossil fuels. These emissions are comparatively small: 20–50 Tg C yr^{-1} for biomass burning and 50–100 Tg C yr^{-1} for fossil fuel use (Collins et al., 1997; Brasseur et al., 1998; Andreae and Merlet, 2001). Sanderson et al. (2003) have provided a breakdown for the H_2 formation from the individual species emitted by these processes; it is reproduced in Table 3. The H_2 emissions from these species total 3.3 Tg H_2 yr^{-1}. They still contain a biogenic component of about 1 Tg H_2/yr—mainly from ethene and propene—as estimated from the precursor emissions given in Collins et al. (1997). Correcting for that the H_2 production for VOC from biomass burning and fossil fuel use amounts to 2.3 Tg H_2 yr^{-1}. It will be adopted here.

The various contributions sum up to 18.1 ± 7 Tg H_2 yr^{-1}. This value can be compared to the previous estimates of the H_2 produced from VOC oxidation listed in Table 1. We note that the present value is somewhat larger than the previous 'bottom up' estimates, which range from 10 to 15 Tg H_2 yr^{-1}. But we also note that each of these estimates has left out one or the other source of VOC considered significant in the current literature on VOC. Novelli et al. (1999) omitted VOC from biomass burning and fossil fuels (the latter was instead included in their industrial surface source of H_2). Sanderson et al. (2003) neglected the monoterpenes and used a much lower CH_3OH emission than currently accepted. Price et al. (2007) included only the emissions of C_5H_8, CH_3OH, monoterpenes and acetone and neglected all other emissions. The inclusion of the neglected VOC sources would raise these previous estimates by 2–4 Tg H_2 yr^{-1}, and bring them into quite reasonable agreement with the H_2 production from VOC oxidation of 18.1 ± 7 Tg H_2 yr^{-1} estimated here.

The top down estimates, on the other hand, demand a total photochemical production of 64 and 77 Tg H_2 yr^{-1}, respectively (see Table 1). After the subtraction of the contribution from CH_4, P_{CH_4,H_2} = 23 Tg H_2 yr^{-1}; this leaves a production of H_2 from VOC of 31 and 44 Tg H_2 yr^{-1}, which are hard to reconcile with the present estimate.

There are, in fact, other constraints, which point to a lower H_2 production from VOC than postulated by the top down estimates (see Novelli et al., 1999). As indicated in Section 3.1, only a fraction of 0.37 from the HCHO formed produces H_2, but a fraction of 0.95 produces CO. Thus, for each Tg of H_2, 36 Tg CO are formed via this reaction path. There are independent calculations of the CO production from VOC oxidation. The more recent ones are summarized in Duncan et al. (2007) and include several studies based on inverse 3-D modelling. Inverse modelling of the CO budget should be much more robust than that of the H_2 budget because in the former, the major sink (reaction with OH, ∼90%) is fairly well known, in contrast to H_2 whose major sink—dry deposition—is rather uncertain (see Section 4.2.2). The total atmospheric CO production from CH_4 and VOC in these studies ranges from 1460 to 1650 Tg CO yr^{-1} (Duncan et al., 2007, and references therein). With the conversion factor 1/36, this translates into a range of 40–46 Tg H_2 yr^{-1} for the total photochemical source of H_2—significantly lower than the estimates from Rhee et al. (2006a) and Xiao et al. (2007) listed in Table 1. Two studies calculated the CO produced from VOC oxidation: 673 (Bergamaschi et al., 2000) and 774 Tg CO yr^{-1} (Müller and Stavrakou, 2005). Duncan et al. (2007) themselves give a bottom up estimate of 521 Tg CO yr^{-1}. These translate into H_2 productions from VOC alone of 18.7, 21.5 and 14.5 Tg H_2 yr^{-1}, respectively. All these values agree well with the present estimates for the H_2 production from CH_4 and VOC and speak against the high values from the top down approaches.

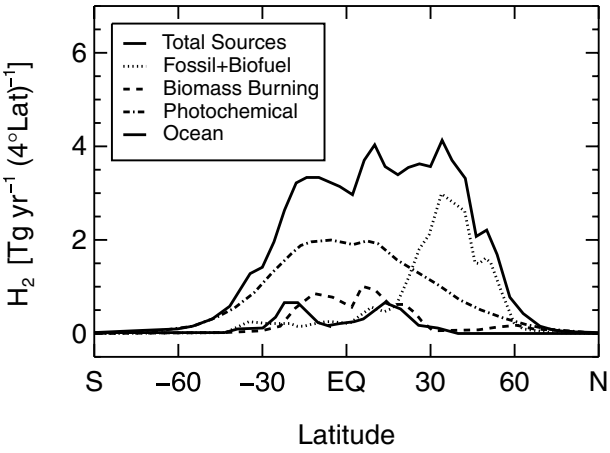

Fig. 6. Latitudinal dependence of major H_2 sources (after Price et al., 2007). The photochemical source refers to the oxidation of all VOC including CH_4; the burning of biofuel is aggregated with fossil fuel use.

Another way of constraining the atmospheric production of H_2 should become feasible in the near future, namely global observations of the HCHO column from satellite. First HCHO fields have already been published (Wittrock et al., 2006), but so far, no attempt has been made to use these to estimate atmospheric H_2 production from HCHO photolysis.

The emissions of biogenic VOC are highly regional and seasonal (Guenther et al., 1995, 2006; see also the monthly, 1° × 1° gridded maps of the emissions of various VOC in the electronic data archives of GEIA/ACCENT (www.aero.jussieu.fr/project/ACCENT/database.php)). Thus, the resulting HCHO fields are highly non-uniform and favour the tropical continents (Wittrock et al., 2006; see also Hauglustaine and Ehhalt, 2002, for modelling results). Modelled fields of the total photochemical H_2 production are given by Price et al. (2007). Their latitudinal and seasonal profiles of the photochemical H_2 production are shown in Figs. 6 and 7. The photochemical H_2 production in Fig. 6 maximizes in the tropics and favours the tropical latitudes of the Southern Hemisphere. This is somewhat at variance with the latitudinal distribution from the 3-D model analysis of Hauglustaine and Ehhalt (2002), which also shows a maximum in the tropics but favours the tropical latitudes of the Northern Hemisphere. In both models, photochemical H_2 production exhibits a strong seasonal maximum in the summer hemisphere.

3.3. H_2 from biomass burning

The surface sources of H_2 are less contentious though not necessarily less uncertain. The two major sources of this type are biomass burning and fossil fuel use. The H_2 emissions from biomass burning listed in Table 1 vary from 12 to 20 Tg H_2 yr^{-1}. Not all of these are original estimates; the highest emission,

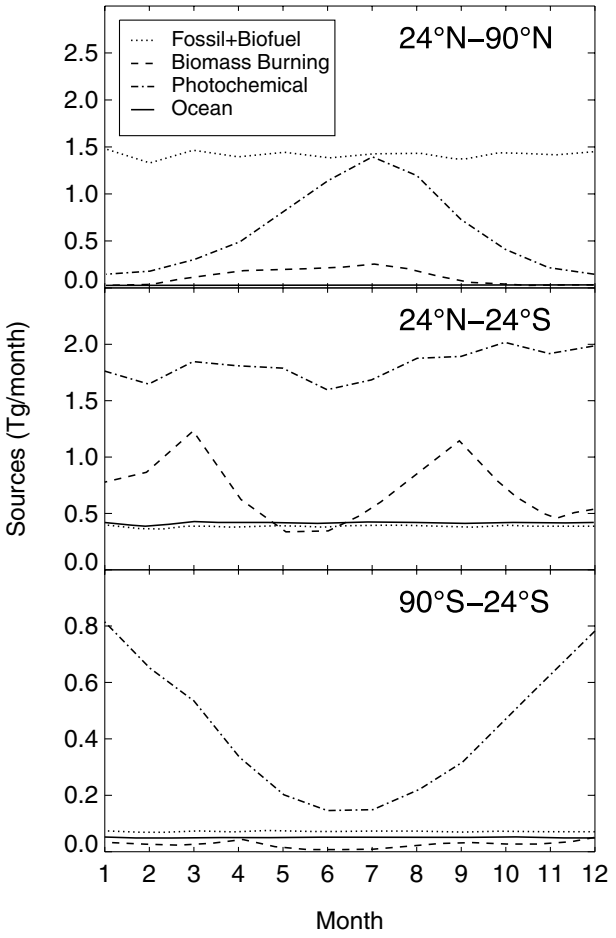

Fig. 7. Seasonal variation of major H_2 sources in three latitude bands (after Price et al., 2007). The photochemical source refers to the oxidation of all VOC including CH_4; the burning of biofuel is aggregated with fossil fuel use.

20 Tg H_2 yr^{-1} (Sanderson et al., 2003) goes back to an earlier estimate by Seiler and Conrad (1987). Apart from the estimates by Rhee et al. (2006a) and Xiao et al. (2007), who used isotope budget analysis or inverse modelling, respectively, the emissions were derived from first estimating the amounts of biomass burned and multiplying these by the appropriate emission factors. The 3-D model analyses by Hauglustaine and Ehhalt (2002) and Price et al. (2007) actually took a short cut. There, the global CO emissions from biomass burning already calculated in the models were multiplied by an average ratio of the H_2 and CO emission factors of 0.28 and 0.29 mol/mol, respectively.

For a more detailed estimate, we turn to Table 4 (excerpted from Andreae and Merlet, 2001). It gives an overview of the different types of burn considered, the amounts of dry matter burned, the emission factors and the resulting direct emissions for H_2 and CO. The various contributions total 15.5 Tg H_2 yr^{-1} (Andreae and Merlet, 2001). This estimate is in good agreement with the value given by Price et al. (2007). This is to be expected, since the latter used the emission factors of Andreae and Merlet (2001), and both groups relied on the same biomass burning statistics of Lobert et al. (1999) and Yevich and Logan (2003). Since these evaluations of biomass burnt and of the emission factors are rather careful and comprehensive, we will adopt the rounded figure of 15 Tg H_2 yr^{-1} as best estimate for the direct emission of H_2 from biomass burning. This estimate includes the contribution from the use of biomass as fuel. It also happens to be close to the average of the biomass emissions reported in Table 1.

The uncertainty of this bottom up estimate depends on the uncertainty in the emission factors and the uncertainty in the amounts of biomass burned. Table 4 gives an indication of the error in the emission factors. In this context, we note that H_2 emission factors were measured only for the first three types of burn and at a few sites only. The emission factors for the others are extrapolated from the average H_2 to CO emission ratio of the first three and the CO emission factors that had been determined for all varieties of biomass burn. From the errors listed in Table 4, we assume an average error in the H_2 emission factor of about 35%.

The amount of biomass burnt annually is also still uncertain. Schultz et al. (2008) provide a discussion of the problems involved. They also quote four studies for the year 2000, which report annual emissions of total carbon released in wild land fires varying between 1428 and 2254 Tg C yr^{-1}. This indicates an error in the annual carbon emission of about 20%, which should also approximate the uncertainty in the amount of dry matter burnt for that category. Here we will apply this error also for the total dry matter burnt annually. Combined with the error in the emission factor, we obtain a total error of 40% or $\pm$ 6 Tg H_2 yr^{-1} for the global emissions of H_2 from biomass burning.

Monthly, $0.5^\circ \times 0.5^\circ$ gridded maps of the emissions of H_2 from biomass burning for the time period 1960–2000 are found in the electronic data archives of GEIA/ACCENT (www.aero.jussieu.fr/project/ACCENT/database.php). These indicate a considerable interannual variability in those emissions—occasionally as large as the error in the estimated average annual emission itself. The latitudinal and seasonal dependence of the H_2 emission from biomass burning are included in Figs. 6 and 7 (after Price et al., 2007).

3.4. *H_2 emissions from fossil fuel use*

This term aggregates H_2 emissions from several technological processes. Most of these also emit CO. This is a consequence of the water–gas shift reaction

$$CO_2 + H_2 \rightleftarrows CO + H_2O, \qquad \text{(R5)}$$

which leaves up to a few per cent of CO and H_2 in the direct hot exhaust of combustion processes. The single most important contribution, about 60% for CO, comes from automobile traffic. Other sources include residential heating, iron and steel industry,

Table 4. Dry matter burned, CO_2, CO and H_2 emissions and emission factors from various types of biomass burning (from Andreae and Merlet, 2001)

		CO_2		CO		H_2	
	Dry matter burned (Tg yr^{-1})	Emissions (Tg CO_2 yr^{-1})	Emission factor (g gas kg^{-1} dry matter)	Emissions (Tg CO yr^{-1})	Emission factor (g gas kg^{-1} dry matter)	Emissions (Tg H_2 yr^{-1})	Emission factor (g gas kg^{-1} dry matter)
Savanna and Grassland	3160	5096	1613 ± 95	206	65 ± 20	3.1	0.97 ± 0.38
Tropical Forest	1330	2101	1580 ± 90	139	104 ± 20	5.1	3.6–4.0
Extratropical Forests	640	1004	1569 ± 131	68	107 ± 37	1.2	1.8 ± 0.5
Biofuel Burning	2701	4187	1550 ± 95	209	78 ± 31	4.8	(1.8)[a]
Charcoal Making	158	70	440	11	70	-	
Charcoal Burning	38	99	2611 ± 241	7.6	200 ± 38	0.17	(4.6)[a]
Agricultural Residues	540	818	1515 ± 177	50	92 ± 84	1.1	(2.4)[a]
Total	8600	13 400		690		15.5	

[a]Extrapolation, based on the average H_2/CO emission factor ratio of 0.32 (molecular units) from savanna and grassland, tropical and extratropical forests.

refineries and fertilizer production (see Duncan et al., 2007 for a more complete list). For all of these, the CO emission factors are known (Duncan et al., 2007). But automobile traffic seems to be the only technological source for which also the H_2 emission factor has been determined. As for biomass burning, the emissions of H_2 from fossil fuel use have been generally obtained by scaling against the better-known CO emissions, using ratios of the H_2 to CO emission factors. All of the H_2 emissions from fossil fuel use in Table 1 have been derived that way, apart from that of Rhee et al. (2006a), which is based on an isotope budget analysis. The numbers range from 15 to 20 Tg H_2 yr^{-1}. Not all of these are independent nor are they calculated on the same basis: Xiao et al. (2007) adopted the earlier estimate of Novelli et al. (1999). The highest estimate of 20 Tg H_2 yr^{-1} (Sanderson et al., 2003) goes back to an earlier estimate by Seiler and Conrad (1987), which may not reflect the general decrease in CO emissions from fossil fuel use since. Hauglustaine and Ehhalt (2002) consider direct emissions only, whereas Novelli et al. (1999) and Price et al. (2007) also include the H_2 produced within the atmosphere from the photo-oxidation of industrial VOC—the latter contributing about 2 Tg H_2 yr^{-1}.

There are also differences in the use of the ratio of the H_2 to CO emission factors. Hauglustaine and Ehhalt (2002) and Price et al. (2007) use a common ratio of 0.588 mol/mol for all types of fossil fuel use, whereas Novelli et al. (1999) differentiate between automobile traffic, with a ratio ranging from 0.49 to 1 mol/mol, and all the others, with a range of 0.06–0.42 mol/mol.

For an update of the H_2 emissions from fossil fuel use, we will follow the approach of Novelli et al. (1999) and use a different ratio for automobile traffic than for the other fossil fuel sources, whose emission ratios appear less well defined. We will, however, only consider direct emissions. The contribution from industrial VOC is already included in our estimate of the H_2 production from the photo-oxidation of VOC (Section 3.2).

Since Novelli et al. (1999), a few more measurements of the H_2/CO ratio of emission factors have been published. They were derived from the slope in the regression line of simultaneously measured H_2 and CO mixing ratios in environments subject to local or regional pollution and are summarized in Table 5 together with the measurements available to Novelli et al. (1999). We note that the H_2/CO ratios measured in the immediate vicinity of car traffic (tunnel, intersection, urban), which are most representative for that source, have relatively high values, whereas more distant environments (suburban, rural) tend to lower ratios; the lowest ratio of 0.15 was reported for the remote station at Mace Head, Ireland. The lower ratios were interpreted as the result of the regional mix of sources and were used to estimate the regional H_2 emissions of the northeastern United States (Barnes et al., 2003) and Europe (Simmonds et al., 2000; Steinbacher et al., 2007). We would like to add a word of caution. The locally measured correlation between two trace gases also depends on their respective lifetimes, which in the case of H_2 and CO differ by about a factor of 10. The effect of this dependence is invariably that the relative variance of the shorter lived trace gas is larger than that in the longer lived (see Ehhalt et al., 1998). This tends to flatten the regression line between H_2 and CO and thus leads to an underestimate of the H_2/CO emission factor ratio: the H_2/CO emission factors derived from measurements farther afield have to be regarded as lower limits for the mix of regional sources.

Using the more recent measurements closest to traffic in Table 5, we estimate an H_2/CO emission ratio for automobile traffic of 0.5 mol/mol, to which we assign an error of ± 0.1.

The H_2 to CO emission ratio for the sum of the other sources is more uncertain. It must be lower than that for traffic to produce

Table 5. Molecular ratio of excess H_2 to excess CO, $\Delta H_2/\Delta CO$, measured at various sites subject to air pollution. For comparison, examples of the H_2/CO ratio in the exhaust of internal combustion engines are included.

Site	Time of measurement	$\Delta H_2/\Delta CO$ (ppb/ppb)	Author
Mainz, Germany	May–June 1973	0.43	Schmidt (1974)
Munich, Germany (aircraft sampling of urban plume)	Before 1975	1	Seiler and Zankl (1975)[a]
Boulder, CO (traffic intersection)	1989	0.6 ± 0.1	Novelli et al. (1999)
Tsukuba, Japan	1995	0.5	Y. Tohjima (1997)[b]
Mace Head, Ireland	1994–1998	0.15	Simmonds et al. (2000)
Harvard Forest, MA	1996–1998	0.40 ± 0.05	Barnes et al. (2003)
VW Gasoline engine, uncontrolled		0.35	Lies (1988)
VW Diesel engine, uncontrolled		0.89	Lies (1988)
Dübendorf, Switzerland (suburban)	Nov 2002–Feb 2005	0.33 ± 0.1	Steinbacher et al. (2007)
Gubrist Tunnel, Switzerland	Nov 2004–Jan 2005	0.48 ± 0.12	Vollmer et al. (2007)

[a]quoted in Conrad and Seiler (1980).
[b]quoted by Novelli et al. (1999).

the lower H_2/CO mixing ratio slopes found at the suburban sites. However, it is not clear by how much exactly owing to the different lifetimes of CO and H_2. Assuming the correction for the different lifetimes to be relatively small for the suburban or rural environments, and further assuming that about 60% of the CO is emitted by automobiles, a H_2/CO emission factor ratio of 0.2 ± 0.15 for the other fossil fuel sources would be compatible with the measurements listed in Table 5.

The corresponding global amounts of CO emitted are much better known. Duncan et al. (2007) derived direct CO emissions from traffic of about 240 Tg CO yr^{-1} and about 400 Tg CO yr^{-1} for all fossil fuel use. These numbers are within 10% of the CO emissions used to calculate the H_2 emissions in Table 1 by other authors (Novelli et al., 1999; Hauglustaine and Ehhalt 2002; Price et al., 2007). We therefore adopt these numbers here too. Earlier estimates gave a wide range of 200–1000 Tg CO yr^{-1} for the global emission of CO from fossil fuel use (see Olivier et al., 1999, for a summary). To accommodate these, we allow an error of 30% for both emission rates. From these CO emissions and the H_2/CO ratio of emission factors given above, we calculate a total H_2 emission from fossil fuel use of about 11 ± 4 Tg H_2 yr^{-1}, of which about 9 ± 3 stem from automobile traffic. This is somewhat lower than the earlier estimates in Table 1 owing to its lower emission factors and the fact that it includes only direct emissions.

There are processes that produce H_2 with little or no CO and are highly local, and thus, might not be captured in the small selection of H_2/CO measurements listed in Table 5. A very important process of this kind is H_2 production from steam reforming of natural gas. It dominates the total industrial H_2 production of about 50 Tg H_2 yr^{-1} (IEA 2003). Losses of more than 1%, which are not inconceivable (Schultz et al., 2003), would lead to a significant release of >0.5 Tg H_2 yr^{-1} to the atmosphere. The possible consequences of a major H_2 economy are taken up in Section 6.

H_2 from fossil fuel use is mostly emitted in the Northern Hemisphere (see Fig. 6) and shows little variation with season (see Fig. 7). Owing to emission controls in cars and industry, as well as technological changes such as the switch from town gas to natural gas in the late 1960s and early 1970s, H_2 emissions from fossil fuel use in the developed countries should have decreased in the latter part of the last century. However, the industrial development of southeast Asia has resulted in a regional increase of CO emissions (see Duncan et al., 2007), which may be paralleled by emissions of H_2.

3.5. H_2 from nitrogen fixation

Biological fixation of atmospheric N_2 is a widespread process carried out by symbiotic and free living bacteria. It is accomplished by the enzyme nitrogenase, which catalyses the reduction of N_2 to NH_3. H_2 is the obligate by-product of that N_2 fixation (for details see Burns and Hardy, 1975). Many of the N_2 reducing bacteria have developed hydrogenase enzymes to recycle the H_2 so formed within the cell. However, for Rhizobium, the important N_2 fixation bacteria contained in the root nodules of legumes, H_2 recycling is rare, and in this case, much of the H_2 formed is released into the surrounding soil. Some of that H_2 escapes uptake by soil and eventually reaches the atmosphere (Conrad and Seiler, 1980). From measurements over clover fields near Mainz, Germany, these authors derived H_2 release rates to the atmosphere up to

10×10^{-8} cm^3 H_2 cm^{-2} s^{-1}. The release rates were highly seasonal and peaked in spring. From these release rates and the N_2 fixation rates by legumes in various ecosystems—agricultural and otherwise—Conrad and Seiler (1980) estimated a global release rate of 2.4–4.9 Tg H_2 yr^{-1}. This is the basis for most of the subsequent estimates of the H_2 emissions from N_2 fixation on land—usually given as 3 ± 2 Tg H_2 yr^{-1}.

Price et al. (2007) prefer to neglect this source, based on the argument that most of that H_2 would be consumed within the soil. In support, they quote the work by McLearn and Dong (2002). This work, however, merely states that elevated H_2 concentrations in soil air increase the microbial capability in the soil to take up H_2. It does not investigate the escape of H_2 to the atmosphere. In view of the directly measured release of H_2 from clover fields by Conrad and Seiler (1980), we prefer to retain the former estimate of 3 ± 2 Tg H_2 yr^{-1} for the global release of H_2 from N_2 fixation on land. We note in passing that this source may have changed with time, for instance, due to the increased cultivation of legumes.

The oceans also act as a source of atmospheric H_2. This observation goes back to the studies by Williams and Bainbridge (1973), Schmidt (1974), Seiler and Schmidt (1974) and Herr and Barger (1978), which reported that ocean surface waters were supersaturated in H_2 with respect to atmospheric H_2 concentrations. An overview of the H_2 content in ocean surface waters is found in Schmidt et al. (1980). In the North and South Atlantic, where most of the measurements were made, the H_2 content averaged 27 nL H_2 (STP)/L H_2O. Extrapolating this H_2 content to all oceans and using a thin film model by Broecker and Peng (1974), several authors (Schmidt, 1974; Seiler and Schmidt, 1974, and Schmidt et al., 1980) estimated the global H_2 emissions from the oceans to 2–4 Tg H_2 yr^{-1}. The range is due to different assumptions about the solubility of H_2 in seawater and, particularly, about the average thickness of the film. These estimates form the basis for all ocean emissions of H_2 published before 2006.

Seiler and Schmidt (1974) also speculated that the oceanic H_2 originated from microbial activities. In fact, a large part must come from nitrogen fixation by cyano bacteria in the ocean. This insight forms the basis of the estimate by Price et al. (2007). From a global oceanic N_2 fixation rate of 150 ± 50 Tg N yr^{-1} (Deutsch et al., 2007) and a stoichiometry of 1 : 1 for the moles of H_2 produced per N_2 fixed after Brock and Madigan (1991), they estimated a H_2 production within the oceans of 11 ± 4 Tg H_2 yr^{-1}. A good part of that H_2 is consumed within the oceans by hydrogenases. Assuming an internal loss of 45%, they estimated an emission of 6 Tg H_2 yr^{-1} to the atmosphere.

The difference to the earlier estimate can be largely reconciled when we observe that the measurements of the H_2 content in the North and South Atlantic missed the areas of major N_2 fixation, which are located in the subtropics (see Deutsch et al., 2007). Even more important—as Deutsch et al. (2007) point out—is that the Pacific appears to have much higher N_2 fixation rates than the Atlantic. The latter is corroborated to some extent by the measurements of William and Bainbridge (1973), which were made in the South Pacific and showed much higher H_2 contents in the ocean surface water than those in the Atlantic. These measurements had been disregarded by Schmidt et al. (1980), because they had not been related to a common standard. They had been related, however, to the H_2 concentration in local air, which must have been close to 0.5 ppm (Williams and Bainbridge, 1973), so that a calibration error could not account for the large supersaturations found. Thus, taken altogether, it is not implausible that the earlier estimates came out somewhat too low.

We, therefore, tentatively accept the estimate of 6 Tg H_2 yr^{-1} by Price et al. (2007). The error in that estimate is large. In addition to the error in the estimate of the oceanic N_2 fixation rate, there is an error in the loss of H_2 within the ocean. To also account for that, we assign an error of ± 3 Tg H_2 yr^{-1} to the global H_2 emissions from the oceans.

The oceanic H_2 emissions map the fields of oceanic N_2 fixation (given in Deutsch et al., 2007). The latitudinal and seasonal profiles of the oceanic H_2 emissions are shown in Figs. 6 and 7 (from Price et al., 2007).

This concludes the list of the major H_2 sources represented in Table 1. There are, however, further processes known to release minor amounts of H_2 into the atmosphere, which have been often overlooked in the published budgets of atmospheric H_2. For completeness, they are addressed briefly in the next section.

3.6. *Minor sources of atmospheric H_2*

These are sources whose emission rates are expected to be less than 1 Tg H_2 yr^{-1}. Usually the rates are highly uncertain, and in some cases, no estimates are available in the refereed literature. One of the longest known sources is the exhalation of H_2 from volcanoes. Its average emission rate has been estimated to 0.2 Tg H_2 yr^{-1} (e.g. Warneck, 1988).

Another process, long known to produce H_2 is fermentation, that is, the breakdown of organic matter under anaerobic conditions. Such conditions are found in waterlogged soils but also in the digestive tracts of animals. Fermentation produces copious amounts of H_2. But most of it is consumed within the relatively closed anaerobic systems themselves, because H_2 serves as substrate for other microorganisms, for instance methanogenic bacteria. Usually, only a small fraction of the H_2 escapes to the atmosphere. As a first guess, we will attempt to estimate the amounts of H_2 reaching the atmosphere from an anaerobic system, by using the sparse information on the H_2/CH_4 ratios in the gas released to the atmosphere and the published global CH_4 emission rate for that process. For instance Conrad and Babbel (1989) have determined the H_2/CH_4 ratio in the gas released from a sample of rice paddy soil to 0.006 mol/mol. This ratio together with a global CH_4 emission rate from rice paddies of about 50 Tg CH_4 yr^{-1} (Prather et al., 2001) gives a H_2 emission

rate of 0.04 Tg H_2 yr^{-1} from that source. Assuming the same H_2/CH_4 ratio for similar systems, such as wetlands, landfills and waste treatment, which have global CH_4 emission rates of about 150, 40 and 20 Tg CH_4 yr^{-1}, respectively, would result in H_2 emissions of 0.11, 0.03 and 0.015 Tg H_2 yr^{-1}.

Some of the H_2 from enteric fermentation can also be estimated in this way. It is excreted through eructation (belching), flatus, but also through breath, because H_2 from the intestines is dissolved in the bloodstream and released through the lungs. Most of the gas released by cattle is excreted via eructation. The eructed gas comes from the rumen and contains about 3‰ H_2 (see Smolenski and Robinson, 1988) and about 25% CH_4 (Moate et al., 1997). Assuming the resulting H_2/CH_4 ratio of 0.012 mol/mol to hold for all ruminants and a global CH_4 emission of 90 Tg CH_4 yr^{-1} (Prather et al., 2001), one obtains a global H_2 emission of 0.14 Tg H_2 yr^{-1} for that source.

The H_2 emission through breath can be estimated more directly. The breath of humans, for example, contains varying amounts of H_2 averaging about 25 ppm (e.g. Sone et al., 2000). With a breathing rate of about 11 kg air d^{-1} for an adult and a population of 6×10^9 one estimates an H_2 release of 0.04 Tg H_2 yr^{-1} from that source. The breath of animals also contains H_2. Assuming similar release rates per body mass, a few tenths Tg H_2 yr^{-1} could be released via human and animal breath.

However, the most important emitters of H_2 from fermentation are, probably, termites. They represent a large biomass, about 670 Tg (cf. Collins and Wood, 1984), and they emit large fractions of H_2 owing to the small size of their digestive tracts. Sugimoto et al. (1998) report H_2/CH_4 ratios of 0.1–10 mol/mol depending on species and diet. Assuming a median ratio of 1 and a global CH_4 emission by termites of 20 Tg CH_4 yr^{-1} (Sanderson, 1996) would result in 2.5 Tg H_2 yr^{-1} released by termites into their immediate environment. A good part of that H_2, which is released into termite nests or underground, is likely to be consumed before it reaches the free atmosphere (see also Section 4.2 on soil uptake of H_2). Nevertheless it is not inconceivable that termites could contribute on the order of 1 Tg H_2 yr^{-1} to the atmospheric H_2 budget. The possibility of termites as source of atmospheric H_2 has been pointed out before by Zimmerman et al. (1982). The maximum H_2 production from termites of 200 Tg H_2 yr^{-1} estimated by these authors is too large, however, to provide a useful constraint.

There are probably further cases of H_2 release from fermentation, for example, from other herbivorous insects. Altogether, H_2 from fermentation may contribute up to a few Tg H_2 yr^{-1} to the atmospheric budget and certainly deserves more study.

In addition to these surface sources, two minor volume sources of atmospheric H_2 can be identified. One is the reaction of excited O atoms (O^1D) from the photolysis of ozone (O_3) with water molecules:

$$O_3 + h\nu \rightarrow O^1D + O_2, \tag{R6}$$

$$O^1D + H_2O \rightarrow OH + OH, \tag{R7a}$$

$$O^1D + H_2O \rightarrow H_2 + O_2. \tag{R7b}$$

Channel (R7a) is the major source of OH radicals in the atmosphere. However, there appears to be a minor channel (R7b), which produces H_2. The yield of that channel has been measured to $(1^{+0.5}_{-1})$% (Zellner et al., 1980) and $(0.6^{+0.7}_{-0.6})$% (Glinski and Birks, 1985; see also Sander et al., 2006). Since (R6) and (R7a) are common reactions—about 1700 Tg O_3 yr^{-1} are destroyed via that path in the troposphere (see Ehhalt, 1999)—one can estimate that about (0.6 ± 0.6) Tg H_2 yr^{-1} could be produced via (R7b) in the troposphere. This reaction is also interesting in so far as it provides another way of producing H_2 in the stratosphere.

The second minor photochemical source of H_2 is the photolysis of glyoxal (CHOCHO):

$$CHOCHO + h\nu \rightarrow HCO + HCO, \tag{R8a}$$

$$\rightarrow H_2 + 2CO, \tag{R8b}$$

$$\rightarrow HCHO + CO. \tag{R8c}$$

Glyoxal is formed in the oxidation of VOC, notably C_5H_8, and in biomass burning. Its column density—observed from satellite—has been shown to average 5% to 10% of that of HCHO over widespread land areas with biogenic emissions (Wittrock et al., 2006). Since the photolysis rate for channel (R8b) equals about that of the corresponding channel (R3b) of HCHO (Saunders et al., 2003) and HCHO from VOC accounts for a H_2 production of about 18 Tg H_2 yr^{-1}, the photolysis of CHOCHO (R8b) could contribute about 1 Tg H_2 yr^{-1}.

There are other minor photochemical reactions leading to the formation of H_2, for example, the decay of excited Criegee radicals formed during the ozonolysis of VOC. The latter, however, has been considered in many of the earlier estimates of H_2 production from VOC and is, at least, incorporated in their error estimates.

Obviously, each of the H_2 sources identified in this section is small compared with the errors in the major sources. They might, therefore, seem negligible. However, these sources could add up to a total that approaches the size of some of the major sources, and it seems important to keep that in mind.

4. Sinks of H_2

The H_2 sources are balanced by two sinks: soil uptake of H_2 and reaction of H_2 with the OH in the troposphere. Because of the very weak vertical gradient in the H_2 mixing ratio in the upper troposphere and lower stratosphere, there is virtually no export of H_2 into the stratosphere. Already the first budget estimates made it clear that soil uptake must be the dominant sink process (Schmidt, 1974). Current estimates place it at about 75% of

the total loss (see Table 1). It is, however, relatively uncertain because of the large variety of soils and biomes that have to be considered. In contrast the loss through reaction with OH is one of the best-known terms of the H_2 budget, and it will be considered first.

4.1. Reaction with OH

This loss mechanism proceeds everywhere in the sunlit troposphere via the reaction

$$H_2 + OH \rightarrow H_2O + H. \quad \text{(R9)}$$

The rate constant, $K_9(T)$, for this reaction and its temperature dependence are well established: $K_9(T) = 2.8 \times 10^{-12} \times \exp(-1800/T)$ molecules^{-1} cm^3 s^{-1}, with an uncertainty of 5% at 298 K and 8% at 272 K (Sander et al., 2006).

The local loss rate is given by

$$L_{H_2,OH} = K_9(T) \times [OH] \times [H_2], \quad (5)$$

where the brackets denote the local number density in units of molecule cm^{-3}.

The annual tropospheric loss rate, $\overline{L_{H_2,OH}}$, is obtained by integration of this product over time and space. 2-D and 3-D models calculate $\overline{L_{H_2,OH}}$ from the generated fields of [OH], [H_2] and K_9(T). Since H_2 is fairly uniformly distributed, an expression analogous to eq. (3) can be used to approximate $\overline{L_{H_2,OH}}$:

$$\overline{L_{H_2,OH}} = K_9(\bar{T}) \times [\overline{OH}] \times \int [H_2] dV. \quad (6)$$

Novelli et al. (1999) used eq. (6) to calculate the tropospheric loss of H_2 due to reaction with OH. With $\overline{[OH]} = (9.7 \pm 0.6) \times 10^5$ cm^{-3} (from Prinn et al., 1995), a reaction constant at 277 K, $K_9(277) = (4 \pm 0.2) \times 10^{-15}$ molecule^{-1} cm^3 s^{-1} and their own estimate for the tropospheric burden of 155 ± 10 Tg, they obtained $\overline{L_{H_2,OH}} = (19 \pm 5)$ Tg yr^{-1}. This estimate agrees well with the $\overline{L_{H_2,OH}}$ calculated by 3-D models, which ranged from 15 to 18 Tg yr^{-1} (see Table 1).

To update the estimate of Novelli et al. (1999), the average of 10.7×10^5 cm^{-3} from Section 3.1 will be used for $\overline{[OH]}$. The updated rate coefficient is $K_9(272) = 3.74 \times 10^{-15}$ molecule^{-1} cm^3 s^{-1} from the $K_9(T)$ given above. The tropospheric burden is 155 Tg from Novelli et al. (1999), applicable even today because of the vanishing trend in global H_2. From these numbers, we obtain $\overline{L_{H_2,OH}} = 19$ Tg yr^{-1}, in good agreement with the previous estimate.

The error of this loss is most readily estimated by recognizing that $\overline{[OH]} \times K(\bar{T}) = \tau^{-1}_{X,OH}$ defines the lifetime, $\tau_{X,OH}$, of a tracer X with respect to its reaction with OH in the troposphere. As a consequence, the lifetimes of two trace gases, for example, H_2 and CH_3CCl_3, scale as $\tau_{H_2,OH}/\tau_{CH_3CCl_3,OH} = K_{CH_3CCl_3OH}(272)/K_8(272)$ (see Prather and Spivakovsky, 1990). The rate constant $K_{CH_3CCl_3,OH}(T) = 1.64 \times 10^{-12} \times \exp(-1520/T)$ molecule^{-1} cm^3 s^{-1} and has an uncertainty of 19% at 272 K (Sanders et al., 2006). As mentioned above, the error in K_8(T) is 8%, and that is also the error of $\tau_{CH_3CCl_3,OH}$ (see Prinn et al., 2005). The quadratic propagation of these errors yields a relative uncertainty for $\tau_{H_2,OH}$ of 22%, which results in an error for $\overline{L_{H_2,OH}}$ of ±5 Tg yr^{-1}, when the error in the tropospheric burden is included. Clearly the error in $\tau_{CH_3CCl_3,OH}$ dominates the error in $\overline{L_{H_2,OH}}$; the latter could be lowered considerably by a more precise measurement of $K_{CH_3CCl_3,OH}$. For future reference, we adopt this value of 19 ± 5 Tg yr^{-1} for the global tropospheric loss of H_2 due to reaction with OH.

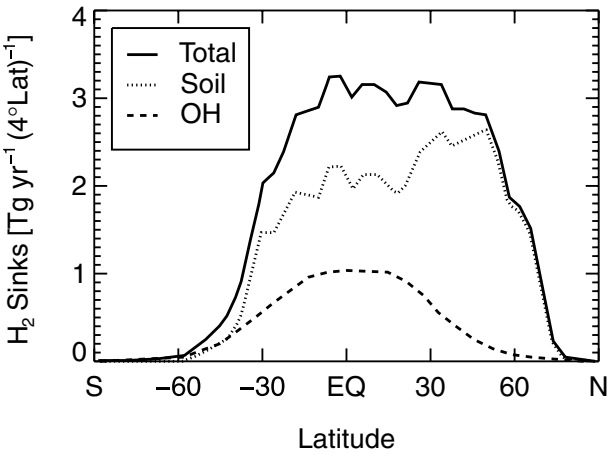

Fig. 8. Latitudinal distribution of the annually averaged sink strengths of H_2 (after Price et al., 2007).

The spatial and temporal distribution of the local loss ($L_{H_2,OH}$) follows closely that of [OH]. As a consequence, it varies strongly with latitude and season. Figure 8 presents the latitudinal dependence of the zonally and annually averaged tropospheric loss of H_2 due to OH in 4° latitude bins. That loss exhibits a broad and pronounced maximum about the equator. Similarly, the seasonal variation of $L_{H_2,OH}$ shows a strong maximum in summer. Examples are found in Hauglustaine and Ehhalt (2002) and Price et al. (2007). Because [H_2] and T decrease with altitude, $L_{H_2,OH}$ is the largest in the lower troposphere (see Schmidt et al., 1980).

4.2. Soil Uptake

Soil uptake is a much larger sink of tropospheric H_2. The current estimates for its global sink strength range from 40 to 90 Tg H_2 yr^{-1} (see Table 1 and references therein). The process is ubiquitous: virtually all investigated soils containing organic carbon were shown to take up H_2. Deposition onto water or vegetation has not been reported. The uptake by soil is probably mediated more by abiontic soil enzymes, that is, by various kinds of hydrogenase attached to soil particles or in dead cells, rather than by the metabolism of living cells (Conrad and Seiler, 1981, 1985; Schuler and Conrad, 1990; Conrad, 1999). In any case, sterilization of the soil by heat or chemicals irreversibly

destroys its capability for H_2 uptake. The exact origin and characteristics of the soil hydrogenases are not known (Gödde et al., 2000). Nevertheless, the rate of uptake and its dependence on a number of parameters have been studied by numerous in situ and laboratory experiments.

4.2.1. Deposition velocity: measurements and characteristics. The rate of uptake is usually given as deposition velocity, v_d (cm s^{-1}), such that the flux of H_2 from the atmosphere to the surface, F, is given by

$$F = v_d c \text{ (molecules cm}^{-2}\text{ s}^{-1}\text{)}, \quad (7)$$

where c is the number density of H_2 in surface air. The deposition velocities for H_2 measured in different biomes by in situ experiments varied between 0.01 and 0.1 cm s^{-1} (see Table 6). Whereas laboratory experiments indicated a strong dependence of v_d on both soil temperature and moisture (Liebl and Seiler, 1976; Conrad and Seiler, 1981; Smith-Downey et al., 2006), deposition velocities measured in situ depended little on soil temperature but varied significantly with soil moisture (Liebl and Seiler, 1976; Conrad and Seiler, 1981, 1985; Förstel, 1986; Schuler and Conrad, 1991; Yonemura et al., 1999; Yonemura et al., 2000b). The soil moisture acts in two ways: apparently a minimum of water is required to keep the soil enzymes active (Conrad and Seiler, 1981; Gödde et al., 2000; Yonemura et al., 2000a). On the other hand, higher amounts of soil water tend to decrease v_d, since a higher amount of soil water reduces the volume of air filled soil pores and separates the pores by water meniscuses, thus lowering soil diffusivity and preventing H_2 from reaching the active sites. Indeed, in laboratory experiments, Conrad and Seiler (1981) demonstrated that the H_2 uptake increased from 0 at a soil moisture around 0% w/w (weight H_2O/weight soil) to a maximum value at a soil moisture around 10% w/w. The uptake rate then decreased to 0 at 30% w/w and 23% w/w soil moisture for samples of aeolian sand and loess loam, respectively. Similar laboratory results were obtained by Smith-Downey et al. (2006) on soils from boreal forest and desert ecosystems. Field experiments—for the most part made at temperate latitudes—-showed a strong anticorrelation between soil moisture and v_d (Förstel, 1986; Förstel and Führ, 1992; Yonemura et al., 1999; Yonemura et al., 2000b), because the soils generally retained a moisture content above 10% w/w.

The experiments further revealed that the uptake of H_2 proceeded within the topmost few centimetres of the soil (Liebl and Seiler, 1976; Förstel, 1986; Yonemura et al., 1999), and that there existed a compensation point at a H_2 mixing ratio of about 50 ppb, below which the uptake of H_2 ceased (Liebl and Seiler, 1976; Conrad and Seiler, 1985; Schuler and Conrad, 1990).

Based on these general observations and his own laboratory studies, Yonemura et al. (2000a) proposed a two-layer soil diffusion model for the uptake of H_2. The upper layer acts essentially as diffusion barrier. It is assumed to be devoid of hydrogenase activity—its thickness, of the order of 1 cm, increasing with dryness. In the layer below, both diffusion and removal of H_2 take place. The model appears to describe reasonably well the observed features of H_2 uptake in temperate zones, such as dependence on soil porosity and moisture. The model also predicts a decrease of the H_2 concentration with depth in the top soil layer, in agreement with the H_2 profiles in soil air measured by Liebl and Seiler (1976) (Interestingly, for some soils, the measured H_2 concentration increased with greater depth to a few 1000 ppb at depths below about 20 cm),

The dependence on soil moisture should lead to significant changes of the H_2 deposition velocity with season, in a number of climate zones. In temperate zones with annually uniform or preferential winter precipitation, we expect a seasonal variation in v_d, with a minimum in winter due to the higher soil moisture content during winter. In colder climates, snow adds a substantial diffusion barrier. Moreover, when the soil is frozen, much of the water is bound as ice, and as in the case of extreme dryness, little liquid water is left to support the soil enzyme activity. In analogy, we would expect H_2 uptake to vanish for soil temperatures significantly below 0°C. Such a decrease has indeed been demonstrated (Smith-Downey et al., 2006). Both effects tend to increase the amplitude in the seasonal variation of v_d with increasing latitude.

There are only a few experimental studies of v_d covering a full year, and some of them report indeed strong seasonal variations: in situ experiments on grass plots in the vicinity of Mainz, Germany, in 1978 and 1979, observed a seasonal variation with a broad maximum of about 0.07 cm s^{-1} between May and October and a minimum of 0.026 cm s^{-1} between December and February (Conrad and Seiler, 1980). Similarly Förstel (1986; 1988) found strong seasonal variations in v_d for pasture and agricultural land in the vicinity of Jülich, Germany, except that the winter minima were more than a factor of 10 lower than the summer values. The deposition velocity appeared strongly anticorrelated with soil moisture throughout the whole year, and the author assigned the low v_d values in winter to the high soil moisture, which came close to saturation, and to occasional frost. These measurements were made on soil samples taken as undisturbed as possible to the laboratory and exposed to tritiated hydrogen gas, HT. Interestingly, forest soil samples taken during the same period and treated in the same manner showed only relatively small fluctuations in v_d throughout the year and no systematic seasonal variation at all. At the same time, the annually averaged v_d of about 0.15 cm s^{-1} for forest soil was much higher than the values for pasture and agricultural land. Part of the difference is probably due to the fact that the forest soil was stripped of its uppermost layer of dead leaves before exposing it to HT (Förstel, personal communication, 2006). For the uptake of CO, it has been shown by in situ experiments that the removal of leaves from the forest floor results in an increase in v_d from 0.027 to 0.038 cm s^{-1}, that is, by a factor of 1.4 (Sanhueza et al.,

Table 6. Dry deposition velocities of H_2 measured in the field on soils of various ecosystems, where available type of soil and vegetation, temperature and season are also listed

Ecosystem	Location	Vegetation	Soil	Season	Soil temperature °C	Deposition velocity (10^{-2} cm s^{-1}) Mean	(Range; summer average)	Reference
Desert	Karoo, South Africa	Semi desert	Sandy sierozem	February 1982		1		Conrad and Seiler, 1985
	Namib Naukluft Park, Namibia	Desert	Sandy sierozem	February 1982		1.60		Conrad and Seiler, 1985
Savannah	Transvaal, South Africa	Grass	Sandy loam	February 1983	25°–40°	13.1	(12–14)	Conrad and Seiler, 1985
Temperate grass and shrubland	Vicinity of Mainz, Germany	Grass	Aeolian sand	November 1974	3°	4.5	(3.8–5.2)	Liebl and Seiler, 1976
	Vicinity of Mainz, Germany	Grass	Tschernosem	December 1974	8°	6.9		Liebl and Seiler, 1976
	Vicinity of Mainz, Germany	Grass	Loess loam	December 1974	5°	7.2		Liebl and Seiler, 1976
	Vicinity of Mainz, Germany	Grass	Loess loam	May 1975	11°	4.2		Liebl and Seiler, 1976
	Vicinity of Mainz, Germany	Grass	Loess loam, loess	Full year 1978,1979 average		5.3	(2.6–8.8; 7)	Conrad and Seiler, 1980
	Vicinity of Mainz, Germany	Clover	Loess loam, loess	Full year 1978, 1979 average		4.4	(2.6–9.6; 7)	Conrad and Seiler, 1980
	Vicinity of Jülich, Germany	Pasture				1.3	(0.4–2.2)	Schmidt et al., 1980
	Vicinity of Jülich, Germany	Pasture	Parabraunerde	September 1985	∼16°	2.6		Förstel, 1986
	Vicinity of Jülich, Germany	Pasture	Parabraunerde	Full year 1986 average		2.5	(0–9; 2.9)	Förstel, 1988
	Wisconsin	Wet boreal lowland		Annual average		1 1		Hurst et al., 1996 quoted in Novelli et al., 1999
	Seattle, University of Washington Campus, 48°N	Lawn		Aug.–Sept. 1998	∼20°	4.25		Gerst and Quay, 2001
	Seattle, University of Washington Campus, 48°N	Lawn		July 1977				Gerst and Quay, 2001
	Helsinki, Finnland, urban park	Grass?		Aug.–Sept. 2005	18°	4.6		Lallo et al., 2006
	Helsinki, Finnland, urban park	Grass?		December 2005	−0,5° to + 5°	2.4		Lallo et al., 2006
Forest	Vicinity of Mainz, Germany	Pine	Aeolian sand	November 1974	5°	10.7		Liebl and Seiler, 1976
	Vicinity of Mainz, Germany	Beech	Loess loam	November 1974	6.5°	6.7		Liebl and Seiler, 1976
	Vicinity of Mainz, Germany	Beech	Loess loam	May 1975	13°	7.6		Liebl and Seiler, 1976
	Vicinity of Jülich, Germany	Deciduous				5.25	(2.1–8)	Schmidt et al., 1980
	Vicinity of Jülich, Germany	Deciduous	Parabraunerde	September 1985	∼16°	11		Förstel, 1986
	Research Center Jülich, Germany	Beech	Pseudogley	Full year 1985		15	(6–22)	Förstel, 1988 Förstel and Führ, 1992

Table 6. Cont'd

Ecosystem	Location	Vegetation	Soil	Season	Soil temperature °C	Deposition velocity (10^{-2} cm s^{-1}) Mean	(Range; summer average)	Reference
	Tsukuba, Japan, 36 °N	Deciduous	Andisol Hydric, Hapludands	Full year 1996–1997, average	3°–25°	6.3	(6–8)	Yonemura et al., 2000b
	Seattle, Washington Park, arboretum	Coniferous	Indianola	July 1999	15°	5.8		Gerst and Quay, 2001
	Delta Junction, Alaska, 63°E48'N	Mature boreal		July 2001		7.3		Rahn et al., 2002
	Delta Junction, Alaska, 63°E48'N	blue spruce						Rahn et al., 2002
	Delta Junction, Alaska, 63°E48'N	Boreal, recent burn		July 2001		4.4		Rahn et al., 2002
	Delta Junction, Alaska, 63°E48'N	Willow, quaking aspen						Rahn et al., 2002
	Loppi, Finnland		Peat	Sept.–Nov. 2005	17°–5°	4.3	(3.5–5.1)	Lallo et al., 2006
	Washington State						(2–6)	Dayalu et al., unpub;
						1		cited in Price et al., 2007
Agricultural Land	Vicinity of Mainz, Germany	bare	Aeolian sand	November 1974	3°	4.4	(3.4–5.2)	Liebl and Seiler, 1976
	Vicinity of Mainz, Germany	Bare	Aeolian sand	April 1975	27°	8.4		Liebl and Seiler, 1976
	Vicinity of Mainz, Germany	Bare	Clay	Nov.,Dec. 1974	5°–9°	3	(2.2–3.8)	Liebl and Seiler, 1976
	Vicinity of Mainz, Germany	Bare	Clay	April 1975	3°	6		Liebl and Seiler, 1976
	Vicinity of Mainz, Germany	Bare	Tschernosem	May 1975	21°	5.6		Liebl and Seiler, 1976
	Vicinity of Jülich, Germany					2	(0.3–3.6)	Schmidt et al., 1980
	Andalusia, Spain	Unplanted	Loamy sand	September 1982	20°–60°	3.3		Conrad and Seiler, 1985
	Vicinity of Jülich, Germany		Parabraunerde	September 1985, average	0.5°–18°	1.7		Förstel, 1986
	Vicinity of Jülich, Germany			Full year average 1984–1985		1.7	(0–7; 2.9)	Förstel, 1986
	Vicinity of Jülich, Germany		Parabraunerde	Full year 1986 average		2.5	(0–10; 3)	Förstel, 1988
	Tsukuba, Japan	Vicia villosa, and bare	Andisol Hydric Hapludands	July–August, 1995	25°–35°	5.1	(0–10; 5.1)	Yonemura et al., 1999
						5.1		
	Tsukuba, Japan	Fallow	Andisol Hydric Hapludands	full year average 1996–1997	0°–30°	4.6	(0–9; 6)	Yonemura et al., 2000b
Peat, tundra	Mace Head, Ireland	Grass	Peaty soil	May 1996	18°	2.6		Simmonds et al., 2000

1998). Assuming that this factor also applies in the present case of H_2 deposition, the annually averaged v_d for the undisturbed forest floor should have been 0.11 cm s^{-1}, still a comparatively high value, even for forest soils (see Table 6). The only other annual study of forest soil was made in situ by Yonemura et al. (2000b) at Tsukuba, Japan, who reported a lower annually averaged uptake of 0.063 cm s^{-1}. The study also found relatively small fluctuations in v_d with a range of 0.05–0.08 cm s^{-1} throughout the year and the absence of a systematic seasonal variation already observed by Förstel (1986; 1988).

Yonemura et al. (2000b) also made measurements of v_d on arable land, which gave an annual average v_d of 0.043 cm s^{-1}. These measurements showed large fluctuations over a range from virtually 0 to 0.09 cm s^{-1} and exhibited a more complex seasonal pattern with possibly two minima, one in March and April and the other in September and October, and two rather sharp maxima, just prior to the minima. The anticorrelation of v_d with moisture was also not as clear-cut as that found for arable land near Jülich, but was rather limited to periods with a steady trend in soil moisture, which indicates that there must be soil parameters other than moisture that influence v_d.

This concludes the short list of annual measurements of v_d available in the literature. They are included along with soil type and temperature in Table 6. We note that these measurements were all made in temperate latitudes and are obviously insufficient to estimate the annual uptake rates for other climates and biomes. For the latter some in situ data on v_d exist, which were taken over shorter periods—usually not more than a month during summer or growth period. In most instances, they are not accompanied by soil moisture measurements. These data are also summarized in Table 6.

A comparison of the data in Table 6 reveals that the uptake rates of temperate forest soils are significantly higher than those of temperate grass and agricultural land. This point is emphasized by the studies that investigated these ecosystems under otherwise similar conditions, that is, same soil, region and season (Liebl and Seiler, 1976; Förstel, 1986; Yonemura et al., 2000b). The uptake rates of agricultural and grass land seem not to differ significantly. There is also an indication in the data from Liebl and Seiler (1976) that v_d may be larger over aeolian sand than over clay, that is, a tentative indication of a dependence of v_d on pore size, which would not be unexpected.

Even with the inclusion of all current field data, the global extent of measured deposition velocities is sparse. Moreover, there is still a lack of controlled field and laboratory experiments to systematically characterize the processes determining v_d of H_2. As a consequence, there is no general algorithm which relates v_d for H_2 to soil conditions. This lack of information still leaves considerable latitude in the extrapolation to a global average. Accordingly, there is a large scatter in the estimates of the global uptake rate of H_2 by soil, and the errors quoted are often large. The older estimates ranged from 20 to 120 Tg H_2 yr^{-1} (Schmidt, 1974; Liebl and Seiler, 1976; see Warneck, 1988, for a summary). They were based on the then available local uptake rates (see Table 6) and the global areas of the respective biomes. Some provided for snow cover, but the dependence on soil moisture or temperature was not considered.

4.2.2. Current estimates of the global uptake of H_2 by soil. The estimates from the last 10 yr are summarized in Table 1. Some of these are based on 3-D models, which in principle are capable of considering maps of soil type, snow cover, surface temperature and soil moisture to yield spatial and seasonal distributions of soil uptake and thus, a more refined estimate of the global uptake rate of H_2. That capability, however, was not fully utilized. For computational economy, shortcuts and simplifications were introduced instead. For example, the first geographical distributions of v_d for H_2, which were provided by the 3-D model analysis of Hauglustaine and Ehhalt (2002), relied on v_d fields of CO already existing in the model for ozone and related chemical tracers (MOZART), whose seasonal and geographical variation was defined by the net primary productivity (NPP), and the fact that the deposition velocities of CO and H_2 are linearly correlated with a scaling factor of 1.5 (see Yonemura et al., 2000b). The resulting global uptake rate of H_2 by soil was 55 Tg yr^{-1}, well within the range of the other estimates (see Table 1).

Even the most recent 3-D model study of the atmospheric H_2 cycle (Price et al., 2007) utilized only snow cover and a coarse gradation of surface temperature to simulate the spatial and seasonal dependence of soil uptake. It assumed an empirical but uniform $v_d = 3.94 \times 10^{-2}$ cm s^{-1} over non-snow covered land at temperatures above 0°C, half that value where temperatures are between 0°C and –15°C and a quarter of that value at temperatures below –15°C. The base value of v_d, 3.94×10^{-2} cm s^{-1}, was selected for optimum simulation of the mean surface observations of H_2. The global uptake rate by soil calculated by this model, 55 Tg yr^{-1}, is, thus, not independent of the choice of the source strengths. A sensitivity study varying the strength of the soil sink by ±15% allowed to place error bars of ±8.3 Tg yr^{-1} on that value. This model simulates the observed latitudinal, vertical and seasonal variation of the tropospheric H_2 mixing ratio quite well. It also captures the observed latitudinal and vertical gradient in the D-content of atmospheric H_2.

The only 3-D model study that explicitly used data from Table 6 was that by Sanderson et al. (2003). It assigned empirical v_d values to seven different ecosystems, and used the empirical, linear dependences of v_d on soil moisture to generate geographic and seasonal changes in v_d. Soil moisture and snow cover, whose impact on v_d was also accounted for, were calculated in the model. The model, thus, accounts for the essential dependences of v_d found in field experiments, namely on snow cover, soil moisture and vegetation type. It, so far, provides the most detailed and realistic estimate of global H_2 uptake by

soil: 58.3 Tg H_2 yr^{-1}. Equally important, the soil sink was not scaled to match the total sources, but represents an independent estimate. Owing to the fact that the model was not run quite to steady-state—the total sources, 78.2 Tg H_2 yr^{-1}, exceeded the total sinks, 74.4 Tg H_2 yr^{-1}—the actual global soil uptake should probably be raised to a steady-state value of 61.3 Tg H_2 yr^{-1}. Unfortunately, the authors did not present the geographical distribution or the seasonal variation of the so derived fields of v_d. The modelled seasonal variations in the concentration of atmospheric H_2 agreed quite well with those measured at comparable surface sites by Novelli et al. (1999).

In addition to these bottom up approaches, which relied to some extent on the measured v_d, isotope analysis of atmospheric H_2 affords an independent top down assessment of the global uptake of H_2 by soil. From a global balance of the deuterium content in the sources and sinks of H_2, Rahn et al. (2003) estimated that soil uptake constitutes a fraction of (77 ± 20)% of the total H_2 loss (see also Section 5.1.2). The central value corresponds to an absolute loss rate of 63 Tg yr^{-1}, when 19 Tg yr^{-1} is used for the global destruction of H_2 by reaction with OH. The uncertainty of this estimate is, however, very large.

In another analysis based on the seasonal variation of the D content in the Northern Hemisphere, Rhee et al. (2006a) derived a global uptake rate of H_2 by soil of 88 ± 11 Tg yr^{-1}. To do so, they had to make a variety of simplifying assumptions, whose uncertainties were not always included in the estimated error. In particular, they assumed that the seasonal increase in the D-content of the Northern Hemisphere can be modelled by a Rayleigh type loss process of tropospheric H_2. This model, however, is only applicable if there are no simultaneous sources. As a consequence of the actual presence of sources, the apparent fractionation factor derived by the authors is not merely given by the fractionation of the sink processes but also depends on the D-content of the sources. This dependence not only lowers, somewhat, the derived combined fractionation factor of the sinks, which in turn lowers the estimated global soil uptake, but, in particular, it increases the uncertainty of the latter substantially above the value given above.

Finally, there is a first attempt at inverse modelling (Xiao et al., 2007). It relies on a Kalman filter in a 2-D 12-box model (Prinn et al., 2001) and on the seasonal variations in atmospheric H_2 observed at four surface stations of the Advanced Global Atmospheric Gases Experiment (AGAGE), one in each of the surface boxes. The optimal estimation provides a value for the annual mean soil uptake in each of the four lowest boxes (heights at 500 hPa; latitude ranges: 90°N–30°N, 30°N–0°, 0°–30°S, 30°S–90°S) which add up to a global uptake rate of 84 ± 8 Tg yr^{-1}.

Thus the recent estimates of global H_2 uptake by soil cluster around two distinct values, namely around 86 Tg yr^{-1} (Rhee et al., 2006a; Xiao et al., 2007) and around 55 Tg yr^{-1} for the others (Hauglustaine and Ehhalt, 2002; Rahn et al., 2003; Sanderson et al., 2003; Price et al. 2007; as well as for the earlier values also given in Table 1). For the former, the errors quoted are relatively small, for the latter, the errors, where quoted, are large—with the exception of the estimate by Price et al. (2007).

The two values are clearly not compatible. Future research is needed to resolve the reasons for the difference.

For the moment, however, we would like to note that one of the high estimates, namely that by Rhee et al. (2006a), has probably a much larger error than quoted by the authors. It, thus, may not differ significantly from the lower value. We further note that the authors of the high estimate from inverse modelling (Xiao et al., 2007) assumed the seasonal variations in the latitude bands 90°N–30°N and 30°N–0° to be equal in amplitude and phase. Given the dependence of v_d on snow cover, soil moisture and temperature, one would expect a much weaker seasonal variation in the tropical latitude band than at the latitudes north of 30°N, which indeed has been found by other authors (see Section 4.2.3). Since the seasonal variations in the atmospheric H_2 mixing ratio are quite sensitive to that of the soil uptake (Hauglustaine and Ehhalt, 2002; Price et al., 2007), the assumption of a seasonal variation independent of latitude within the Northern Hemisphere could have introduced a bias in the mean uptake rate. Moreover, as noted in Section 3.2, the larger soil sink requires larger sources to maintain the tropospheric burden. The calculations by inverse modelling suggested an increased H_2 production from VOC oxidation. The same was assumed by Rhee et al. (2006a) to close the H_2 budget. This explanation, however, appears untenable in view of the excessive and incompatible impact the concurrent CO production would have on tropospheric CO budget. Given these caveats, we prefer the rounded value of 60 Tg yr^{-1} suggested by the bottom up estimate by Sanderson et al. (2003) as the current best estimate for the globally averaged soil uptake rate. It must, however, have a large uncertainty given the large variability in the measured v_d. To accommodate the high estimates, an asymmetric error of +30/–20 Tg yr^{-1} is assigned to the global soil uptake rate.

4.2.3. Seasonal and latitudinal distribution of soil uptake. Some models also report seasonal variation and spatial distribution of the soil uptake. Figure 9 summarizes the published information of the seasonal variation averaged over the Northern Hemisphere. All these variations show the expected form: high uptakes in summer, when soils are warm and dry, and low values in winter, when soils are cool and wet. At the same time, the curves differ slightly in phase, but considerably in amplitude. This is a consequence of the various assumptions made in the calculation of the soil uptake. The NPP assumed by Hauglustaine and Ehhalt (2002) to define the seasonal and spatial distribution of the dry deposition velocity (v_d) does not necessarily reflect the strong control by soil moisture (and texture). Thus, that assumption is likely to result in an inadequate parametrization, especially of the seasonal variation in v_d. In fact, from a detailed comparison of modelled and measured seasonal variations in atmospheric H_2 at a number of surface stations, the authors concluded that the use of NPP leads to an underestimate of v_d

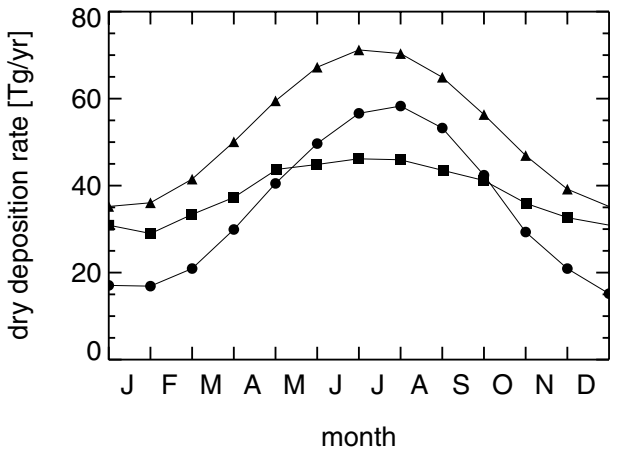

Fig. 9. Seasonal variations of the H_2 dry deposition rate in the Northern Hemisphere (0°–90°N latitude) from recent models using different approaches. Full circles: Based on the geographical distribution of continental net primary productivity (Hauglustaine and Ehhalt, 2002). Full squares: Based on a coarse gradation of the seasonal temperature distribution and snow cover (adapted from Price et al., 2007). Full triangles: Based on inverse modelling using the seasonal variation in H_2 at the four AGAGE surface stations (adapted from Xiao et al., 2007). For details see text.

during winter and spring over the continents in the Northern Hemisphere.

The seasonal variation derived from inverse modelling (Xiao et al., 2007) exhibits the highest uptakes in all seasons. As already indicated in the previous section, that result could be influenced by the assumption that the seasonal variations in the latitude bands 90°N–30°N and 30°N–0° are equal in amplitude and phase, which is highly unlikely. In fact, the temperature- and snow-cover-dependent parametrization of v_d by Price et al. (2007) gave a strong average seasonal variation in the soil uptake at latitudes between 24°N and 90°N, but virtually no variation with season in the tropical, 24°N–24°S, and southern, 24°S–90°S, latitude bands.

From those variations and a weighting factor determined from their latitudinal dependence of soil uptake (Price et al., 2007, see Fig. 8), one can also derive a seasonal variation of soil uptake averaged over the full Northern Hemisphere, 0°–90°N. That variation is included in Fig. 9 and probably represents the most realistic of the three seasonal variations shown there. There is room for improvement, though. None of the models represented in Fig. 9 has made full use of the existing field and laboratory observations of the dependences of v_d, in particular, none considered its soil moisture dependence, although this seems within the capability of current modelling (Sanderson et al., 2003). A state of the art parametrization of v_d should include its dependence on snow cover and frost, a classification according to soil types or biomes and the empirical dependence on soil moisture, including the decrease in v_d for very dry soils observed in laboratory studies.

Price et al. (2007) also calculated the latitudinal dependence of the soil uptake. This dependence is included in Fig. 8. In contrast to the removal by OH reaction, the other tropospheric sink of H_2, soil uptake is asymmetric about the equator and strongly favours the Northern Hemisphere, as to be expected from the land mass distribution. Moreover, at nearly all latitudes soil uptake substantially exceeds the removal of H_2 by OH. Thus, on annual average about two-third of the total destruction of H_2 reside in the Northern Hemisphere (a fact already noted by previous authors e.g. Novelli et al., 1999). A latitudinal dependence of soil uptake was also published by Hauglustaine and Ehhalt (2002), together with global maps of v_d for summer and winter.

5. Isotopic composition of atmospheric hydrogen

The element hydrogen has three isotopes: protium ($^1H = H$), the most abundant isotope; deuterium ($^2H = D$), twice as heavy and much rarer, and tritium ($^3H = T$), the radioactive isotope of hydrogen. Tritium is a weak beta emitter with a half-life of 12.32 yr. All three isotopes occur naturally in atmospheric H_2. Because of the relative rarity of the heavier isotopes, they are present essentially in the form of HD and HT. Their abundances are usually given as ratio, D/H and T/H, relative to the main isotope. The large relative mass differences between the H isotopes lead to large fractionations in the chemical reactions processing H_2 in the atmosphere, a fact that adds to the usefulness of D and T as tracers for the atmospheric H_2 cycle.

5.1. *D content in atmospheric H_2*

The D/H ratio or D content is generally measured masspectrometrically, relative to a standard. As a consequence, it is expressed as deviation (δ) in per million (‰) from that standard—usually SMOW with a D/H ratio of $(155.76 \pm 0.06) \times 10^{-6}$ (Hageman et al., 1970; see also Craig, 1961):

$$\delta_{Sa} = [(R_{Sa} - R_{SMOW})/R_{SMOW}] \times 1000, \quad (7)$$

where R = D/H, and the indices refer to sample (Sa) and standard (SMOW).

5.1.1. Spatial and temporal variation in the D content. Atmospheric H_2 has an unusually high D content. Already its first measurement—made pycnometrically on water from the combustion of H_2 in the raw neon fraction from an air liquefaction plant at Hamburg-Wilhelmsburg—indicated a D content that was substantially higher, namely (25 ± 7)%, than that of local surface water (Harteck and Suess, 1949). This meant—as the authors immediately recognized—that atmospheric H_2 could not be in thermodynamic equilibrium with water vapour or other H containing molecules. That would lead to a very low D content

in H_2. Thus, the authors concluded that atmospheric H_2 must be subject to a cycle of continuous production and removal, involving substantial isotope fractionations. At the time the escape of H atoms from the earth's uppermost atmosphere was favoured, as explanation for the D enrichment in atmospheric H_2.

Raw neon samples were also used subsequently, mainly from 1955 to 1965, to analyse the D and T content of atmospheric H_2 (Begemann and Friedman, 1959, 1968; Gonsior and Friedman, 1962; Ehhalt et al., 1963; 1966; Ehhalt, 1966; Gonsior et al., 1966; Bainbridge et al., 1961). The samples came essentially from five locations: Buffalo, NY; and Hamburg, Lohhof, Ludwigshafen, Oberhausen, all in Germany; and were collected irregularly over varying time periods. The longest and best-sampled series is that from Lohhof, which lasted from February 1962 to June 1965. The D measurements were made massspectrometrically and were much more precise than the first measurement from 1949. Nevertheless, most data sets showed a large scatter, because the air liquefaction plants providing the samples were usually located in industrialized areas and, thus, were subject to contamination from local or regional H_2 sources with low D content. Altogether, the observed D contents ranged from –300‰ to 180‰ in the SMOW scale. D and T content were well correlated, indicating that the contaminant H_2 had a low D and T content compared to that of average atmospheric H_2. The correlation allowed to extrapolate the D content of the contaminant H_2. It generally varied between -200‰ and -330‰ and was thought to be largely due to car exhaust (Gonsior et al., 1966). An exceptional value of -600‰ found in Lohhof appeared to be caused by contamination from a nearby H_2 production plant (Ehhalt et al., 1966). Where simultaneous measurements of the H_2/He or H_2/Ne ratio were available, such as for Lohhof and Oberhausen, the D content was also well correlated with the H_2/He ratio. Extrapolation to the lowest H_2/He ratio yielded a D content of 80‰ for the background atmospheric H_2 (Ehhalt, 1966). This value was corroborated by the measurements of Friedman and Scholz (1974), who installed a small air liquefaction device on Mount Evans, 4300 m above sea level and about 45 km west of Denver, CO, for the collection of H_2 samples from the free troposphere. The data collected between November 1967 and June 1969 allowed to deduce a D content of (70 ± 30) ‰ for atmospheric H_2 in clean air.

Recent D measurements of H_2 are much more numerous, made at cleaner sites and provide a broad picture of the spatial and temporal variation of the D content in atmospheric H_2: clean air samples from surface stations, ship cruises and aircraft campaigns gave an average D content of about 130‰ (Gerst and Quay, 2000; see also Gerst and Quay, 2001; Rahn et al., 2003; Rhee et al., 2006a; Price et al., 2007). This value is significantly higher than those from the 1960s and indicates an increase in the D content of atmospheric H_2. This increase is probably real and caused, to a large part, by the increase in tropospheric CH_4, whose photo-oxidation produces H_2 with a high D content (see below).

The recent data clearly show an interhemispheric gradient—with the D-content in the Southern Hemisphere higher by 15‰ (Gerst and Quay, 2000; Rhee et al., 2006a; Price et al., 2007).

Price et al. (2007) also report a seasonal variation (2002–2005) in the D content of H_2 at the Cheeka Peak Observatory, WA (48°N, 124°W)—about sinusoidal in form and a minimum of 94‰ in April and a peak of 118‰ in fall. A seasonal variation with similar phase, but smaller amplitude and larger mean value of 128‰, has been deduced by Rhee et al. (2006a) from H_2 samples obtained during three aircraft transects in May, July and December 2000 for the upper troposphere, from about 10°N to 40°N. The corresponding seasonal variation in the Southern Hemisphere from about 10°S to 30°S showed a maximum in February and a minimum in August and a similar peak-to-peak amplitude of 8‰.

The most conspicuous feature in the temporal and spatial distribution of the D content in atmospheric H_2, however, is a strong vertical increase in the stratosphere from 130‰ at the tropopause to about 400‰ at 32 km altitude (Rahn et al., 2003; Röckmann et al., 2003). The samples were collected by Rahn et al. (2003) from the NASA ER-2 aircraft in January–March 2000, between 65°–80°N,13°–63°E and 11–21 km altitude and by a balloon launched on 24 October 2002 over Aire sur l'Adour, France, 43.7°N, by Röckmann et al. (2003). At even higher altitudes, 44–62 km, a D content of 310‰ had been obtained from a whole air sample collected by a rocket-borne cryogenic sampler on 24 September 1968, over White Sands, NM, 31°N (Ehhalt and Volz, 1976; see also Ehhalt et al., 1975).

In contrast, the vertical gradient in the troposphere—so far only obtainable as difference of surface measurements and data in the upper troposphere—appears very weak.

5.1.2. The D budget of tropospheric H_2. The average D content of tropospheric H_2 is a result of the tropospheric HD budget. It is given by the isotopic balance eq. (8):

$$\sum_i R_{s_i} s_i = \sum_j R_{l_i} l_i, \tag{8}$$

where the annually and globally averaged D/H ratios of the source and loss terms are given by R_{s_i} and R_{l_j}, respectively, and the s_i and l_j are the averaged source and loss rates of tropospheric H_2. Temporary trends in H_2 and D, which are currently negligibly small, are omitted. The losses all operate on tropospheric H_2. Thus, the right-hand side of eq. (8) can be written as

$$\sum_i R_{s_i} s_i = \sum_j \alpha_j l_i R_t, \tag{9}$$

where R_t is the average D/H ratio of tropospheric H_2 and the $\alpha_j = l_{\mathrm{D}j}/l_j$ are the ratios of the global loss rates of the isotopic molecules HD and H_2. The α_j are identical to the so-called fractionation factors, which are given by the ratio of the rate constants of the isotopic to normal H_2 molecules for the various loss processes and have been measured independently

Table 7. Globally averaged D-contents of H_2 from tropospheric sources (units: ‰ SMOW) and average fractionation factors of the major tropospheric sink processes by various authors. Bold numbers indicate the values adopted as current best estimates

	Gerst and Quay 2001	Rahn et al. 2002b, 2003	Rhee et al. 2006a	Price et al. 2007
Troposheric H_2	**130 ± 4**‰	120‰	132‰	130‰[a]
Source:				
Fossil Fuel	−196 ± 10‰	**−270**‰	−270‰[b]	−196‰[a]
Biomass Burning	**−290 ± 60**‰	−290‰[a]	−90‰	−290‰[a]
N_2 fixation, Ocean		−700‰[c]	−700‰[d]	**−628**‰[e]
N_2 fixation, Land		**−700**‰[c]	−700‰[d]	
Photochemical production from CH_4		213^{+264}_{-228}‰[p]	190 ± 50‰[f]	
Photochemical production from VOC				
Photochemical production, total	130 ± 70‰[g]	213^{+264}_{-228}‰[h]	190±50‰[h]	**162 ± 57**‰[i]
Fractionation Factor:				
Soil uptake, α_{soil}	**0.943 ± 0.024**	0.94	0.943[a]	0.926[j]
Oxidation by OH, α_{OH}	0.606 ± 0.019[k]			
	0.595 ± 0.043[l]	0.56[m]	0.58[n]	0.568[o]

[a]from Gerst and Quay, 2001.
[b]from Rahn et al., 2002.
[c]assuming thermodynamic equilibrium between H_2 and H_2O.
[d]from Rahn et al., 2003.
[e]from Rice and Quay, in preparation 2006.
[f]from Rhee et al., 2006b.
[g]from closure of tropospheric HD budget.
[h]assumes D-content of H_2 from photochemical production of total VOC to equal that of D-content of H_2 from photochemical production from CH_4.
[i]from closure of 3-D model.
[j]modified from Gerst and Quay, 2001.
[k]room temperature, Ehhalt et al., 1989.
[l]room temperature, Talukdar et al., 1996a.
[m]280 K, Talukdar et al., 1996.
[n]277 K, Talukdar et al., 1996.
[o]average tropospheric temperature, Talukdar et al., 1996.
[p]error propagated from fractionation factor $\alpha_{CH4-H2} = 1.33^{+0.29}_{-0.25}$.

(see Table 7). Using the balance equation for ordinary H_2,

$$\sum_i s_i = \sum_j l_i, \tag{10}$$

and introducing

$$\frac{\sum s_i R_{s_i}}{\sum s_i} = \overline{R_s} \tag{11}$$

for the mean D content of the source terms,

$$\frac{\sum \alpha_j l_{j_i}}{\sum l_i} = \overline{\alpha_l} \tag{12}$$

for the mean fractionation factor of the sink terms, eq. (9) can be simplified to

$$\overline{R_s} = \overline{\alpha_l} R_t \tag{13}$$

or in δ notation:

$$1 + \overline{\delta_s} = \overline{\alpha_l}(1 + \delta_t). \tag{14}$$

Today, there exist estimates for most of the terms entering in the D budget eq. (8). The various estimates for the loss and production terms of tropospheric H_2, l_j and s_i are listed in Table 1. We note, however, that the D budget requires one more loss and source term than the H_2 budget, namely the exchange of HD between troposphere and stratosphere. Because the H_2 mixing ratios in the troposphere and stratosphere are virtually equal the loss of H_2 to the stratosphere, l_{t-s}, and the import of H_2 from the stratosphere, s_{s-t}, are also equal and cancel in the H_2 budget. In the D budget, however, they are weighted by the different D contents of tropospheric and stratospheric H_2, and $\delta_{st} s_{s-t} \neq \delta_t l_{t-s}$. Assuming a stratospheric residence time of 2.5 yr (Rahn et al., 2003; cf. Holton, 1990), an average tropopause altitude of 12 km (200 hPa) and a tropospheric H_2 burden of 150 Tg (see Table 1), we obtain $s_{s-t} = l_{t-s} = 15$ Tg H_2 yr^{-1}. The D content of stratospheric H_2 was given by Rahn et al. (2003) to $\delta_{st} =$ 200‰; it corresponds to the vertically averaged D content of the stratospheric H_2 column.

The most recent estimates of the globally averaged δ values for the other tropospheric H_2 sources are summarized in Table 7, which also contains the fractionation factors α_i. The fractionation factor for the exchange with the stratosphere, $\alpha_{t-s} = 1$, by definition, since the tropospheric H_2 transported into the stratosphere retains its D content. The respective measurements of the other fractionation factors, α_{OH} and α_{soil}, are in good agreement (Ehhalt et al., 1989; Talukdar et al., 1996, respectively, Ehhalt et al., 1989; Gerst and Quay, 2001; Rahn et al., 2002a). In contrast, the various δ values of the sources still show considerable scatter. We further note that the D content of some of the sources, for example, biomass burning, N_2 fixation on land and photochemical oxidation of VOC, will vary geographically with the D content of the plant material it is derived from. This in turn depends on the D content of local water, which decreases systematically with increasing latitude and altitude (Schiegl and Vogel, 1970), because the heavier isotopes are preferentially depleted during precipitation. The surface sources of H_2 are all more or less depleted in D. In contrast, H_2 resulting from the photochemical destruction of CH_4 exhibits a relatively large positive δ. This was first realized by Gerst and Quay (2001), who noted that the successive steps of H abstraction from the CH_4 molecule would result in a H_2CO molecule enriched in D, which upon photolysis would yield H_2 enriched in D (the oxidation chain of CH_4 is given in Mar et al., 2007). They further solved balance eq. (8) for the δ value of H_2 from the CH_4 oxidation, using the s_i, l_j from the budget of Novelli et al. (1999) and the δ values of the other sources listed in the second column of Table 7 and obtained (130 ± 70) ‰. This value actually represents the average over all sources whose δ value could not be specified at the time, that is, it includes the oxidation of VOC, oceanic and terrestrial nitrogen fixation and the input from the stratosphere. Nevertheless, since the surface and stratospheric sources are smaller and partially cancel, this δ value served to demonstrate that the photochemical oxidation of VOC and CH_4 must produce H_2 with a positive δ value.

This result was corroborated by Rahn et al. (2003), who derived the fractionation factor for H_2 produced from the oxidation of CH_4, $\alpha_{CH_4-H_2} = 1.33^{+0.29}_{-0.25}$, from the vertical decrease of the D content in stratospheric H_2 and a box model balancing the local H_2 produced from CH_4 against the H_2 lost through reactions with OH, O^1D and Cl. The fractionation factors for the loss reactions, $\alpha_{OH} = 0.51$, $\alpha_{O1D} = 1$ and $\alpha_{Cl} = 0.52$, were taken from Talukdar and Ravishankara(1996), Talukdar et al. (1996) and Taatjes (1999), respectively. Rahn et al. (2003) further assumed that this stratospheric $\alpha_{CH_4-H_2}$ also applied to the troposphere. With an average D content of –86‰ for tropospheric CH_4 (Quay et al., 1999) this yields a D content of 216‰ for tropospheric H_2 produced from CH_4. The D content of 213‰ given by Rahn et al. (2003) and listed in Table 1 is based on a D content for CH_4 of –90‰. With somewhat different approaches and assumptions and a slightly faster increase in the D content of stratospheric H_2, Röckmann et al. (2003) and Rhee et al. (2006b) obtained (180 ± 50)‰ and (190 ± 59)‰, respectively, for the D content of tropospheric H_2 from CH_4. Although these estimates agree reasonably well, their uncertainties remain quite large.

In a recent paper, Mar et al. (2007) carefully reviewed the information available on the isotopic fractionations in the various oxidation steps of CH_4, leading to H_2. With a sensitivity analysis based on a 2-D model, they showed that this information places relatively loose constraints on the overall kinetic fractionation $\alpha_{CH_4-H_2}$. They further showed that $\alpha_{CH_4-H_2}$ must vary with latitude and altitude and concluded that the average mass weighted D content in H_2 from CH_4 oxidation in the troposphere could well be higher than that derived for the stratosphere and range from 220‰ to 340‰.

In the meantime, measurements on some of the missing kinetic fractionation factors have been published. Nilsson et al. (2007) reported the HCHO and HCDO yields in the reaction of CH_2DO with O_2; they found a branching ratio of 88.2% for HCDO and 11.8% for HCHO. Feilberg et al. (2007) and Rhee et al. (2007) measured the fractionations in the photolysis of HCHO and HCDO for conditions at the earth's surface. Unfortunately, the measurements do not agree. For the overall photolysis rates, J, Feilberg et al. (2007) found a ratio $J_{HCDO}/J_{HCHO} = 0.63$ whereas Rhee et al. (2007) found $J_{HCDO}/J_{HCHO} = 0.40$. For the photolysis into the molecular channel, Feilberg et al. (2007) obtained a ratio $J_{HCDO-HD+CO}/J_{HCHO-H_2+CO} = 0.55$, Rhee et al. (2007) a value of 0.50, and for the photolysis into the radical channel, the former reported a ratio of $(J_{HCDO\rightarrow H+DCO} + J_{HCDO\rightarrow D+HCO})/J_{HCHO\rightarrow H+HCO} = 0.91$ versus 0.22 by Rhee et al. (2007). We also note that these newly measured fractionation factors for the photolysis of HCHO fall outside the ranges considered by Mar et al. (2007). Since much of the overall fractionation combined into $\alpha_{CH_4-H_2}$ depends on the fractionations occurring in the production and destruction of HCHO the new photolysis data so far rather add to the uncertainty of $\alpha_{CH_4-H_2}$.

The D content of H_2 from the photochemical destruction of VOC has not yet been determined. In some studies, it has been assumed to equal that from the photochemical destruction of CH_4 (Rahn et al., 2003; Rhee et al., 2006a). However, the production of HCHO from VOC oxidation, for instance from C_5H_8, proceeds largely without abstraction of H atoms. The HCHO so produced could be much less enriched in D than HCHO from CH_4 and so would be the eventually resulting H_2. The other approach, in which a combined D content for H_2 from CH_4 and VOC oxidation was derived as balance from the isotopic budget (Gerst and Quay, 2001; Price et al., 2007; see Table 7), remains somewhat uncertain, as long as the D content of all other sources are not established.

For some of the remaining sources, the δ values listed in Table 7 differ so much that they are hard to reconcile, and one has to make a choice which to adopt as global average.

For H_2 from fossil fuel combustion there are two recent values: –196‰ (Gerst and Quay, 2001) and –270 ‰ (Rahn et al.,

2002b). The difference is probably due to the fact that the two estimates consider different mixes of combustion sources. The first value is based on three samples from a parking garage and, thus, specific for passenger cars under slow driving conditions. The second estimate is based on a reasonable number of measurements in metropolitan environments (Los Angeles Basin). It includes direct measurements of car exhaust, which ranged from –91‰ to –310‰. This second estimate is much more likely an average over contributions from a variety of vehicles under all driving conditions, as well as contributions from stationary fossil fuel combustion and other anthropogenic sources. We, therefore, adopt –270‰ for the average D content of anthropogenic H_2 emissions.

For H_2 from biomass burning we adopt –290‰ (Gerst and Quay, 2001). This value was derived from laboratory experiments measuring the D fractionation during smouldering and flaming combustion and extrapolated to a global value using the globally averaged D content of plant matter ($\delta = -80$‰). The competing value of –90‰ (Rhee et al., 2006a) was derived much more indirectly from measurements of the D content of H_2 in the upper troposphere invoking numerous assumptions.

For H_2 from N_2 fixation in the ocean, we adopt the δ value of –628 ‰, which apparently is based on measurements (see Price et al., 2007). Earlier Luo et al. (1991) had measured a D content of –600‰ in H_2 photoproduced by cyanobacteria—the available water having a D content of –7‰, that is, close to that of sea water.

Owing to the lower D content of continental freshwater, N_2 fixation on land could well yield H_2 with a D content of –700‰ as estimated by Rahn et al. (2003) based on the assumption of thermodynamic equilibrium between substrate and evolving H_2.

For completeness, we also list the few available measurements of the D content in minor sources of H_2: H_2 from the volcano Surtsey, Iceland, $\delta = -110$‰ to –150‰ (Arnason and Sigurgeirsson, 1968); H_2 emitted by Termites, $\delta = -778$‰ (Rahn et al., 2002b); H_2 in swamp gas, $\delta = -690$% (Rahn et al., 2002b).

Given the large uncertainties remaining, the constraints provided by the D budget for the tropospheric H_2 cycle are still somewhat weak. Nevertheless, it holds great promise, and eq. (12) has been used to estimate the global strength of the soil sink (Rahn et al., 2003; Rhee et al., 2006a), whose uncertainty is especially large and cumbersome to improve on by local measurements (see Section 4.2.2).

Moving beyond such box model analyses, Price et al. (2007) utilized the recently discovered spatio-temporal features in the D content of H_2, such as the mean latitudinal gradient or seasonal variation, in a 3-D model analysis to further constrain the H_2 budget. Their H_2 and HD budget generate most features in the observed spatio-temporal distribution of tropospheric H_2 and its D content. Their globally averaged budget terms are listed in Table 7 and Table 1 (see also Section 6).

5.2. *T content*

Atmospheric H_2 contains T in very low ratios. These are often expressed in Tritium Units, TU, where 1 TU corresponds to a T/H ratio of 10^{-18}. The T content is measured by low-level β counting (see Östlund and Mason, 1974, for experimental procedures). The current T content in tropospheric H_2 is about 2×10^5 TU. A very small fraction of the T is natural—produced by the interaction of cosmic rays with atmospheric oxygen and nitrogen (Craig and Lal, 1961; Lal, 2002)—the overwhelming part comes from various man-made sources. The fraction of natural T in H_2 is poorly quantified. Even the first measurements of T in H_2 made in 1949, which averaged about 5×10^3 TU (Faltings and Harteck, 1950; Fireman and Rowland, 1961), probably suffered from some degree of anthropogenic contamination. This number, therefore, can only serve as upper limit for the natural T content of tropospheric H_2.

5.2.1. Trend in HT. In the years following 1949, the T content in H_2 rose nearly exponentially to 5×10^5 TU in 1959 (see Martell, 1963; Ehhalt, 1966, for summaries). All these measurements including those made through 1967 were made on H_2 samples recovered from air liquefaction plants that were also used for D analysis (Begeman and Friedman, 1959; Gonsior, 1959; Bishop and Taylor, 1960; Gonsior and Friedman, 1962; Ehhalt et al., 1963, 1966; Gonsior et al., 1963, 1966; Friedman and Scholz, 1974; Bainbridge et al., 1961).

In 1968, Östlund and Mason started a program using a different sampling technique that measured HT regularly at a number of surface stations (Östlund and Mason, 1974). The measurements at Miami are published until 2002, so that a fairly complete history of the T content in tropospheric H_2 can be constructed (Happell et al., 2004). It shows that the T content continued to increase reaching a broad maximum of about 2.6×10^6 TU in 1975. From then on, it decreased nearly exponentially to 2.3×10^5 TU in 2002 (Happell et al. (2004) and all other publications from this group use the unit (T/mg air) for the HT mixing ratio. To convert it to a T/H ratio, we assumed a H_2 mixing ratio of 530 ppb).

5.2.2. HT emissions. From the trend of the tropospheric T content in H_2, Happell et al. (2004) constructed the history of the HT inventory, and with a tropospheric lifetime of H_2 of 2.1 yr and the appropriate fractionation, factors the HT emission history. Correlating the temporal development of the HT emissions with the history of various nuclear activities, Happel et al. (2004) proceeded to identify the major sources of tropospheric HT: (1) accidental release associated with increasing production and handling of T for the development of thermonuclear bombs in the 1950s; (2) venting of HT from underground tests in the USA and the USSR from the late 1950s to the early 1990s and (3) release of HT from the nuclear power industry beginning in the 1970s but dominating only since 1990.

The direct injection of T through atmospheric thermonuclear explosions 1952–1963, the largest source of T in the atmosphere,

seems to have contributed relatively little HT. Most of that T ended as HTO owing to the presence of a large excess of O_2. Its contribution to HT has never been quantified. We note, however, that the H_2 in the air collected between 44 km and 62 km altitude in September 1968 by a rocket borne sampler had a T content of 17×10^6 TU (Martell and Ehhalt, 1974). This is much higher than the T content in troposperic H_2 at the time, which was about 2×10^6 TU. Thus, it appears that at least at high altitudes some of the bomb injected T had been converted to HT.

The stratospheric HT content in that sample is also of interest because it was accompanied by the measurement of the HTO mixing ratio of 9.7×10^3 T/mg air in the same air sample. Assuming a mixing ratio of water vapour of 5.5 ppm that HTO mixing ratio converts to a T/H ratio in water vapour of $(43 \pm 15) \times 10^6$ TU (Ehhalt et al., 2002). This value indicates that at that time, about 5 yr after the last large injections, HT and HTO were relatively close to isotopic equilibrium—in contrast to stratospheric HD and HDO, which are quite far from it (see also Section 5.1.1).

5.2.3. Vertical and latitudinal distribution of HT. The work of Östlund and Mason (1974) also provided some information on the latitudinal and vertical distribution of HT mixing ratio in the troposphere. Despite considerable scatter, their data can be used to derive average gradients. The vertical gradients observed seemed to vary year-to-year and with location.

For February 1971, at 70°–75°N, north of Alaska, Östlund and Mason (1974) report an HT profile, which decreased from about 4×10^6 TU in the upper troposphere to 2×10^6 TU in the lower stratosphere.

In late winter and spring 1972, the mean of several profiles indicate a uniform T/H ratio of about 2×10^6 TU between 5 and 14 km altitude over the central USA (Mason, 1977). In late winter 1973 and 1974, the mean profile showed a slight increase from 1.8×10^6 TU at 7 km to 2.2×10^6 TU at 12 km in the upper troposphere over the central USA. That increase continued into the stratosphere and reached 2.4×10^6 TU at 18 km altitude (Mason, 1977). This variability in the vertical HT gradient was probably typical of the Northern Hemisphere in the 1970s and a result of the local and episodic nature of the injections by under ground tests. It is not expected for today's troposphere.

A latitudinal gradient was observed, both in the upper troposphere by airborne sampling, 1971 and 1972, and at the surface during ship transects, 1974–1976 (Mason, 1977). Both data sets showed higher HT concentrations in the Northern Hemisphere. The data from the upper troposphere give an average T/H ratio for the Northern Hemisphere (38°N–0° latitude) of 2.14×10^6 TU and for the Southern Hemisphere ($0° \times 39°$S latitude) of 1.93×10^6 TU.

From the interhemispheric difference in HT, Mason (1977) estimated a HT lifetime of 6–10 yr for the Southern Hemisphere. Even after accounting for the isotope fractionation in the reaction of HT with OH, this lifetime is too high and too uncertain to provide a useful constraint for the tropospheric lifetime of H_2 (see Ehhalt et al., 1989).

So far not much could be learned for the atmospheric cycle of H_2 from the measurements of its T content—mostly owing to the lack of an independent estimate of the strengths of the man made HT sources. In view of the possibility of future energy production from nuclear fusion reactors, however, the study of the fate of tropospheric HT seems a worthwhile effort.

6. Discussion and summary

Our estimates of the strengths of the major sources and sinks were carried out individually and bottom up, without regard to whether the totals would eventually balance. Nevertheless, the total production rate, 76 Tg H_2 yr^{-1}, closely matches the total loss rate, 79 Tg H_2 yr^{-1}, as it should, considering that the current trend in the tropospheric burden is very small. The difference is well within the error of each of these rates (see Table 1). It even leaves room for a contribution from the minor sources. The precise match in the 3-D analyses or top down approaches in Table 1 is the result of an a priori requirement of steady-state and tuning of one of the source or sink terms to achieve a realistic global distribution in H_2 or its D/H ratio.

The present budget terms agree well with the previous estimates for the total production and loss of tropospheric H_2 from bottom up and 3-D analyses (see Table 1). Actually, already the estimates of the individual source and sink terms are in reasonable agreement, as detailed in Sections 3 and 4. Owing to overlap in the assumptions and approaches, the range in the totals for loss and production listed in Table 1 is less than their individual error estimates would suggest.

This agreement does not extend to the top down approaches based on inverse modelling or HD balance, which indicate a much larger tropospheric turnover of H_2 (Rhee et al., 2006a; Xiao et al., 2007). This large turnover is based on the large global dry deposition rate derived by these authors, which forces a much higher H_2 production from VOC oxidation. For various reasons—notably the constraint placed on H_2 by the CO budget—the large H_2 production from VOC and thus the large turnover seems unlikely (see Sections 3 and 4 for details). We, therefore, favour the lower loss estimate of 79 Tg H_2 yr^{-1}. Together with the tropospheric H_2 burden of 155 Tg H_2 (Novelli et al., 1999), it yields a tropospheric H_2 lifetime of 2 yr.

Most of the tropospheric H_2, namely 60 Tg H_2 yr^{-1}, is removed by dry deposition with about 70% destroyed in the Northern Hemisphere (see Fig. 8). Since soil temperature and, in particular, soil moisture, regulate the uptake rate, global dry deposition may vary with climate and global changes in land use. The photochemical removal of H_2 within the troposphere is comparatively small, 19 Tg H_2 or about 10 Tmol yr^{-1}. Thus, in

photochemical turnover, H_2 ranks only fourth among the oxidizable species, after CO, CH_4 and other VOC with photochemical turnovers of 100 Tmol yr^{-1}, 30 Tmol yr^{-1}, and 15 Tmol yr^{-1}, respectively.

The total sources also favour the Northern Hemisphere, mainly owing to the burning of fossil and bio-fuel (cf. Fig. 6). With about 64%, the excess is not as large as for the total losses. This results in a net deficit in the H_2 balance of the Northern Hemisphere, which maintains the current interhemispheric gradient in the H_2 mixing ratio of about 3% (Novelli et al., 1999; see Section 2).

A fair share of the H_2 sources are under human control. The major anthropogenic contributions come from oxidation of CH_4, whose sources are to about 60% anthropogenic, fossil fuel use, bio-fuel use and part of biomass burning. Today about 50% of the total tropospheric H_2 production can be considered anthropogenic.

Most of the H_2 sources, whether direct or via precursors, are largely controlled by processes residing at the surface, that is, outside the atmosphere. For H_2, the losses are also largely controlled by processes outside the atmosphere, namely, the dominant role of dry deposition. Only the H_2 production from CH_4 and the H_2 destruction by OH can be calculated exclusively from atmospheric information. This means that the mean concentration as well as temporal and spatial distribution of H_2 in the troposphere are largely controlled by the strengths and distributions of surface processes, whose uncertainties are still considerable. This hampers inverse modelling in determining budget terms and limits the usefulness of consistency checks of the H_2 budget by 3-D modelling. In both cases, the outcome rests to some degree on the assumptions made about surface sources and sinks, for example, the exact functional form of the seasonal variation in dry deposition (see Section 4.2, and Fig. 9). Both approaches, therefore, require extensive sensitivity analyses covering the full range of uncertainties in the input parameters to determine the true uncertainty in the target parameter. A point in case is the fact that the inverse model by Xiao et al. (2007) derives a global dry deposition rate of 85 ± 5 Tg H_2 yr^{-1} to match the modelled to the observed seasonal variations in the H_2 concentration at four stations, whereas the 3-D model analysis by Price et al. (2007) achieves a similarly good match at many more stations with a dry deposition rate of 55 ± 8.3 Tg H_2 yr^{-1}.

Some of the H_2 sources must have changed with time, notably H_2 from CH_4 oxidation and fossil fuel use. There is no evidence that this caused a trend in the background H_2 mixing ratio, partly due to the fact that the data before 1985 were too sparse and noisy to detect one and lacked intercalibration (see Section 2.1). The evidence over the last two decades, based on the numerous and well-calibrated measurements of the global CMDL network, indicate that presently there is virtually no trend in the average H_2 mixing ratio (Novelli et al., 1999, see also Section 2.1, Fig. 1).

There is evidence, however, that the interhemispheric gradient in the H_2 mixing ratio has reversed from higher concentrations in the Northern Hemisphere in the early 1970s, to lower concentrations than in the Southern Hemisphere today (see Section 2.3). In addition, the D-content of background H_2 has increased from about 80‰ in the late 1960s to about 130‰ today (see Section 5.1.1). The latter observation indicates that the increase in the H_2 production from CH_4 oxidation has indeed impacted the tropospheric distribution of H_2. There is no answer in the literature to the question why the impact has not been seen in the trend.

Thanks to the work of several global and regional networks and that from individual laboratories, the spatial and temporal distribution of tropospheric H_2 is by now reasonably well known. However, due to differences in analytical methods and calibration, these data cannot be combined. The NOAA GMD measurements provide an internally consistent data set with which to view global H_2. Using 52 surface sites, the tropospheric interhemispheric gradient, its burden and trend have been determined (Novelli et al., 1999; Price et al., 2007; see Section 2 and Figs. 2 and 3): at some typical land and ocean sites vertical profiles covering all seasons are also available (Pak, 2000; Price et al., 2007, see Section 2 and Fig. 4).

This data set allows a rather detailed test of the distributions predicted from 3-D models and thus a consistency check of the underlying H_2 budget, that is, the strengths, as well as the spatial and temporal distributions of sources and sinks. The most recent attempt of this kind is the work by Price et al. (2007). It is also the most comprehensive, as it includes an analysis of the HD budget. The various intercomparisons provided by the authors—mainly in form of figures—show good agreement between the measured and modelled H_2 burden, latitudinal dependence, seasonal variations at numerous stations and vertical profiles. The model also explains the rather more sparse observations on the D content of H_2, namely the average tropospheric D content, its latitudinal gradient and seasonal variation at one station. The agreement of the model results with all the various features in the observed H_2 distribution suggests that the H_2 budget underlying the model is reasonably realistic. However, it does not prove it. The consistency between measured and modelled distribution is a necessary but not sufficient condition. Within the error bounds, the model might reproduce the observed H_2 distribution from other variants of the H_2 budget. However, the increasing variety of observations available for comparison should reduce the probability of a significant departure of the underlying hydrogen budget from reality. Moreover, sensitivity studies can, at least, define the error in that budget. For the single most important and uncertain term in the H_2 budget, the global rate of dry deposition, Price et al. (2007) carried out such a sensitivity test by varying the central value of 55 Tg H_2 yr^{-1} by $\pm$ 15%. To maintain the tropospheric burden, each source was varied by a uniform 11.3%. This change led to changes in both the latitudinal gradient and burden but remained within the observational error

bounds. Changes beyond 15% led to a significant degradation in the agreement between modelled and measured H_2 and allowed to assign an error of ± 15% to this loss. Although still no proof, this test adds evidence in favour of the value of 60 Tg H_2 yr^{-1} for the global dry deposition rate adopted here. The comparison itself also tells us that the choice of budget terms suggested here, which is reasonably close to that of Price et al. (2007), would lead to a modelled H_2 distribution consistent with the observations too.

At this point, it is not clear whether the same is true for the distribution of the D content in tropospheric H_2. Since we prefer to keep the H_2 source from nitrogen fixation on land, the present H_2 budget has higher H_2 emissions from microbial sources than that of Price et al. (2007): 9 Tg H_2 yr^{-1} versus 6 Tg H_2 yr^{-1}. In addition, we raise the possibility of minor H_2 emissions from termites. These additional microbial sources have very low D contents (Section 5; Table 7) and, thus, would significantly alter the HD budget, despite the fact that their H_2 emissions are relatively small. Used together with the choice of D contents for the various H_2 sources from Price et al. (2007), these additional microbial emissions would presumably deteriorate the agreement between modelled and observed distributions of the D content in H_2 found by these authors. On the other hand, there are still quite large ranges in the estimated D contents of most of the sources (Table 7) and a slightly different choice in these contents could easily reconcile the present H_2 budget with the observed distribution of the D content. Given the large uncertainty in the D content of the sources, the constraint on the H_2 budget provided by the distribution of the D content and the HD budget remains weak.

Despite the remaining uncertainties, our knowledge of the tropospheric H_2 cycle is solid enough to make reasonable predictions about the consequences of its perturbation. In fact, such predictions have already been made. They were triggered by the prospect of H_2 as a major energy carrier for industry and traffic and were based on 2-D and 3-D models (Prather, 2003; Schultz et al., 2003; Tromp et al., 2003; Warwick et al., 2004). The assumptions made by the various authors on the share of H_2 in the future total energy consumption and the eventual leakage rates in the H_2 distribution system varied widely: from 50% to 100% of the current fuel use in the former case and from 3% to 20% of the total H_2 used for the leakage rate. As a consequence, the predicted changes in the tropospheric H_2 burden varied widely: from a factor of 1.3 in the more moderate and probably more realistic case (Schultz et al., 2003) to a factor of 4 in the extreme case of high H_2 use and high losses (Tromp et al., 2003). The general consequences for atmospheric chemistry are twofold, a decrease in the tropospheric oxidation capacity owing to a lowering in the average OH concentration and an increase in stratospheric water vapour with possible consequences for stratospheric ozone. As it turns out, for the moderate scenario, the increase in H_2 by itself, which is our primary interest here, has very little impact on tropospheric OH and O_3 (Schultz et al., 2003). In the model, the impact comes through a secondary effect, namely the replacement of fossil fuel, whose combustion emits NO_X and other pollutants, by emission-free H_2, which results in a 5% reduction in tropospheric O_3 and a 6% reduction in OH. The impact on global stratospheric O_3 appears to be small, even in the event of a strong increase in tropospheric H_2 (Warwick et al., 2004). The model calculations by Tromp et al. (2003) suggest, however, that a large increase in H_2 could cause a significant decrease of O_3 in the northern polar vortex.

The prospect of H_2 as a major energy carrier has also increased the general interest in and the amount of work on the atmospheric H_2 cycle. The research community has established new programs such as the European Network for Atmospheric Hydrogen Observations and Studies (EUROHYDROS; http://www.meteor.uni-frankfurt.de/eurohydros) or common platforms such as the forum hydrogen energy chances and risks for the environment (HyCARE), whose workshops summarize the most recent research in that field. Its reports are available at the web page http://www.fz-juelich.de/hycare/.

The two major needs to further constrain the atmospheric H_2 cycle are better estimates for the global rates of soil uptake and of the photochemical production of H_2 from VOC. These are the largest and, at the same time, most uncertain sink and source terms, respectively. The former will need substantial field work on the uptake rates in the most important ecosystems over a full year to define the parameters for regional algorithms which take account of soil structure, moisture and temperature, and from which eventually a complete global picture of soil uptake can be developed. For the latter, there is more immediate hope. As mentioned in Section 3, the tropospheric burden of HCHO may serve as another constraint for the photochemical production of H_2 from VOC. This quantity is already available from satellite observations (Wittrock et al., 2006) and may, in the near future, become precise enough for an accurate estimate of the global production of H_2 from HCHO photolysis, the by far dominant path of H_2 from VOC oxidation. It could, thus, lay at rest the controversy over this large source and remove a great part of the uncertainty in the total sources of H_2.

References

Andreae, M. O. and Merlet, P. 2001. Emission of trace gases and aerosols from biomass burning. *Global Biogeochem. Cycles* **15**, 955–966

Arnason, B. and Sigurgeirsson, T. 1968. Deuterium content of water vapour and hydrogen in volcanic gas at Surtsey, Iceland. *Geochim. Cosmochim. Acta* **32**, 807–813.

Bainbridge, A., Friedman, I. and Suess, H. E. 1961. Isotopic composition of atmospheric hydrogen and methane. *Nature* **192**, 648–649.

Barnes, D. H., Wofsy, S. C., Fehlau, B. P. and Gottlieb, E. W. 2003. Hydrogen in the atmosphere: observations above a forest canopy in a polluted environment. *J. Geophys. Res.* **108**, D6, 4197, doi:10.1029/2001JD001199.

Begemann, F. and Friedman, I. 1959. Tritium and deuterium content of atmospheric hydrogen. *Z. Naturforsch.* **A14**, 1024–1031.

Begemann, F. and Friedman, I. 1968. Isotopic composition of atmospheric hydrogen. *J. Geophys. Res.* **73**, 1139–1147.

Bergamaschi, P., Hein, R., Heimann, M. and Crutzen, P. J. 2000. Inverse modeling of the global CO cycle. *J. Geophys. Res.* **105**, 1909–1927.

Bishop, K. F. and Taylor, B. T. 1960. Growth of the tritium content of atmospheric molecular hydrogen. *Nature* **185**, 26–27.

Bousquet, P., Hauglustaine, D. A., Carouge, C. and Ciais, P. 2005. Two decades of OH variability as inferred by an inversion of atmospheric transport and chemistry of methyl chloroform. *Atmos. Chem. Phys.* **5**, 2635–2656.

Brasseur, G. P., Hauglustaine, D. A., Walters, S., Rasch, P. J., Müller, J.-F. and co-authors. 1998. MOZART, a global chemical transport model for ozone and related chemical tracers, 1: model description. *J. Geophys. Res.* **103**, 28 265–28 295.

Brock, T. D. and Madigan, M. T. 1991. *Biology of Microorganisms* 6th edition (eds. T. Aloisi and C. Bracewell). Prentice Hall, Upper Saddle River, NJ, 604–608.

Broecker, W. S. and Peng, T.-H. 1974. Gas exchange rates between air and sea. *Tellus* **26**, 21–35.

Burns, R. C. and Hardy, R. W. F. 1975. *Nitrogen Fixation in Bacteria and Higher Plants*. Springer Verlag, Berlin, Heidelberg, New York.

Collins, N. M. and Wood, T. G. 1984. Termites and atmospheric gas production. *Science* **224**, 84–86.

Collins, W. J., Stevenson, D. S. and Derwent, R. G. 1997. Tropospheric Ozone in a global-scale three-dimensional Lagrangian model and its response to NO_x emissions controls. *J. Atmos. Chem.* **26**, 223–274.

Conrad, R. 1999. Soil Microorganisms Oxidizing Atmospheric Trace Gases (CH_4, CO, H_2, NO). *Ind. J. Microbiol.* **39**, 193–203.

Conrad, R. and Babbel, M. 1989. Effect of dilution on methanogenesis, hydrogen turnover, and interspecies hydrogen transfer in anoxic paddy soil. *FEMS Microbiol. Ecol.* **62**, 21–28.

Conrad, R. and Seiler, W. 1980. Contribution of hydrogen production by biological nitrogen fixation to the global hydrogen budget. *J. Geophys. Res.* **85**, 5493–5498.

Conrad, R. and Seiler, W. 1981. Decomposition Of atmospheric hydrogen by soil-microorganisms and soil enzymes. *Soil Biol. Biochem.* **13**, 43–49.

Conrad, R. and Seiler, W. 1985. Influence of temperature, moisture, and organic carbon on the flux of H_2 and CO between soil and atmosphere: field studies in subtropical regions. *J. Geophys. Res.* **90**, 5699–5709.

Craig, H. 1961. Standard for reporting concentrations of deuterium and oxygen-18 in natural waters. *Science* **133**, 1833–1834.

Craig, H. and Lal, D. 1961. The production rate of natural tritium. *Tellus* **13**, 85–105.

Deutsch, C., Sarmiento, J. L., Sigman, D. M., Gruber, N. and Dunne, J. P. 2007. Spatial coupling of nitrogen inputs and losses in the ocean. *Nature* **445**, 163–167, doi:10.10.1038/nature05392.

Dlugokencky, E. J., Houweling, S., Bruhwiler, L., Masarie, K. A., Lang, P. M. and co-authors. 2003. Atmospheric methane levels off: temporary pause or a nem steady-state? *Geophys. Res. Lett.* **30**, doi:1029/2003GL018126.

Duncan, B. N., Logan, J. A., Bey, I., Megretskaia, I. A., Yantosca, R. M. and co-authors. 2007. Global budget of CO, 1988–1997: source estimates and validation with a global model. *J. Geophys. Res.* **112**, D22301, doi:10.1029/2007JD008459.

Ehhalt, D. H. 1966. Tritium and deuterium in atmospheric hydrogen. *Tellus* **18**, 249–255.

Ehhalt, D. H. 1999. Gas phase chemistry of the troposphere, in Global aspects of atmospheric chemistry (ed. R. Zellner). *Topics Phys. Chem.* **6**, 21–109.

Ehhalt, D. H. and Tönnißen, A. 1979. Hydrogen and carbon compounds in the stratosphere. In: *Proceedings of the NATO Advanced Study Institute on Atmospheric Ozone: Its Variation and Human Influences* (ed. A. C. Aikin), *Report No FAA-EE-80-20*, Aldeia das Acoteias, Portugal, 1–13 October.

Ehhalt, D. H. and Volz, A. 1976. Coupling of the CH_4 with the H_2 and CO cycle: isotopic evidence. In: *Symposium on Microbial Production and Utilization of Gases (H_2, CH_4, CO)* (eds. H. G. Schlegel, G. Gottschalk and N. Pfennig). Akad. der Wiss. Göttingen, Germany, 23–33.

Ehhalt, D., Israel, G., Roether, W. and Stich, W. 1963. Tritium and deuterium content of atmospheric hydrogen. *J. Geophys. Res.* **68**, 3747–3751.

Ehhalt, D., Roether, W. and Stich, W. 1966. Der Anstieg des Tritiumgehaltes im atmosphärischen Wasserstoff seit 1960. *Z. Naturforsch.* **21a**, 1703–1709.

Ehhalt, D. H., Heidt, L. E., Lueb, R. H. and Martell, E. A., 1975. Concentrations of CH_4, CO_2, H_2, H_2O, and N_2O in the upper troposphere. *J. Atmos. Sci.* **32**, 163–169.

Ehhalt, D. H., Schmidt, U. and Heidt, L. E. 1977. Vertical Profiles of molecular hydrogen in the troposphere and stratosphere. *J. Geophys. Res.* **82**, 5907–5911.

Ehhalt, D. H., Davidson, J. A., Cantrell, C. A., Friedman, I. and Tyler, S. 1989. The kinetic isotope effect in the reaction of H_2 with OH. *J. Geophys. Res.* **94**, 9831–9836.

Ehhalt, D. H., Rohrer, F., Wahner, A., Prather, M. J. and Blake, D. R. 1998. On the use of hydrocarbons for the determination of tropospheric OH concentrations. *J. Geophys. Res.* **103**, 18981–18997.

Ehhalt, D. H., Rohrer, F., Schauffler, S. and Pollock, W. 2002. Tritiated water vapor in the stratosphere: vertical profiles and residence time. *J. Geophys. Res.* **107**, D24, 4757, doi:10.1029/2001JD001343.

Engel, A., Wetter, T., Buchholz, U., Volk, M., Bönisch, H. and co-authors. 2005. Measurements of molecular hydrogen at the Institute for Atmosphäre und Umwelt of the J.W. Goethe University Frankfurt. In: *Proceedings of the first HyCare meeting Hamburg* (ed. M. G. Schultz), Germany, 16–17 December 2004, *Berichte zur Erdsystemforschung* **5**, 20–22.

Fabian, P., Borchers, R., Weiler, K. H., Schmidt, U., Volz, A. and co-authoes. 1979. Simultaneously measured vertical profiles of H_2, CH_4; CO, N_2O, $CFCl_3$, and CF_2Cl_2 in the mid-latitude stratosphere and troposphere. *J. Geophys. Res.* **84**, 3149–3154.

Faltings, V. and Harteck, P. 1950. Tritium content of the atmosphere (Der Tritiumgehalt der Atmosphäre). *Z. Naturforsch.* **5a**, 438–439.

Feilberg, K. L., Johnson, M. S., Bacak, A., Röckmann, T. and Nielsen, J. C. 2007. Relative tropospheric photolysis rates of HCHO and HCDO measured at the European photoreactor facility. *J. Phys. Chem. A* **111**, 9034–9046.

Fireman, E. L. and Rowland, F. S. 1961. An additional measurement of tritium content of atmospheric hydrogen of 1949. *J. Geophys. Res.* **66**, 4321.

Förstel, H. 1986. Uptake of elementary tritium by the soil radiation protection. *Dosimetry* **16**, 75–81.

Förstel, H. 1988. HT to HTO conversion in the soil and subsequent tritium pathway: field release data and laboratory experiments. *Fusion Tech.* **14**, 1241–1246.

Förstel, H. and Führ, F. 1992. Trockene Deposition von Tritium in den Boden. *Forschungszentrum Jülich Annual Report*, pp. 45–51.

Friedman, I. and Scholz, T. G. 1974. Isotopic composition Of atmospheric hydrogen, 1967–1969. *J. Geophys. Res.* **79**, 785–788.

Galbally, I. E. and Kirstine, W. 2002. The production of methanol by flowering plants and the global cycle of methanol. *J. Atmos. Chem.* **43**, 195–229.

Gerst, S. and Quay, P. 2000. The deuterium content of atmospheric molecular hydrogen: method and intitial measurements. *J. Geophys. Res.* **105**, 26 433–26 445.

Gerst, S. and Quay, P. 2001. Deuterium component of the global molecular hydrogen cycle. *J. Geophys. Res.* **106**, 5021–5031.

Glinski, R. J. and Birks, J. W. 1985. Yields of molecular hydrogen in the elementary reactions HO_2+HO_2 and $O(^1D_2)+H_2O$. *J. Phys. Chem.* **89**, 3449–3453.

Glueckauf, E. and Kitt, G. P. 1957. The hydrogen content of atmospheric air at ground level. *Q. J. R. Meteorol. Soc.* **83**, 522–528.

Gonsior, B. 1959. Tritium-Anstieg in atmosphärischem Wasserstoff. *Naturwiss* **46**, 201–202.

Gonsior, B. and Friedman, I. 1962. Tritium und deuterium im atmosphärischen Wasserstoff. *Z. Naturforsch.* **17a**, 1088–1091.

Gonsior, B., Friedman, I. and Ehhalt, D. H. 1963. Measurements of tritium and deuterium concentration in atmospheric hydrogen. *J. Geophys. Res.* **68**, 3753–3758.

Gödde, R., Meuser, K. and Conrad, R. 2000. Hydrogen consumption and carbon monoxide production in soils with different properties. *Biol. Fertility Soils*, **32**, 129–134.

Gonsior, B., Friedman, I. and Lindenmayr, G. 1966. New tritium and deuterium measurements in atmospheric hydrogen. *Tellus* **18**, 256–261.

Guenther, A., Hewitt, C. N., Erickson, D., Fall, R., Geron, C. and co-authors. 1995. A global model of natural volatile organic compound emissions. *J. Geophys. Res.* **100**, 8873–8892.

Guenther, A., Karl, T., Harley, P., Wiedinmyer, C., Palmer, P. I. and co-authors. 2006. Estimates of global terrestrial isoprene emissions using MEGAN (Model of Emissions of Gases and Aerosols from Nature). *Atmos. Chem. Phys.* **6**, 3181–3210.

Haan, D., Martinerie, P. and Raynaud, D. 1996. Ice cor data of atmospheric carbon monoxide over Antarctica and Greenland during the last 200 years. *Geophys. Res. Lett.* **23**, 2235–2238.

Hagemann, R., Nief, G. and Roth, E. 1970. Absolute isotopic scale for deuterium analysis of natural waters: absolute D/H ratio for SMOW. *Tellus* **22**, 712–715.

Happell, J. D., Östlund, G. and Mason, A. S. 2004. A history of atmospheric tritium gas (HT) 1950–2002. *Tellus* **56B**, 183–193.

Harteck, P. and Suess, H. E. 1949. Der Deuteriumgehalt des freien Wasserstoffs in der Erdatmosphäre. *Naturwiss*. **36**, 218.

Hatakeyama, S., Izumi, K., Fukuyama, T., Akimoto, H. and Washida, N. 1991. Reactions of OH with α-pinene and β-pinene in air: estimates of CO production from the oxidation of terpenes. *J. Geophys. Res.* **96**, 947–958.

Hauglustaine, D. A. and Ehhalt, D. H. 2002. A three-dimensional model of molecular hydrogen in the troposphere. *J. Geophys. Res.* **107**, 4330, doi:10.1029/2001JD001156.

Heidt, L. E., Pollock, W. A., Lueb, R. A. and Krasnec, J. P. 1979. Vertical distributions of stratospheric trace gases at northern latitudes, In: *Proceedings of the Symposium on the Budget and Cycles of Trace Gases and Aerosols in the Atmosphere*, Commission on Atmospheric Chemistry and Pollution, 12–18 August 1979, Boulder, CO.

Heikes, B. G., Chang, W., Pilson, M. E. Q., Swift, E., Singh, H. B. and co-authors. 2002. Atmospheric methanol budget and ocean implication. *Global Biogeochem. Cycles* **16**, 1133, doi:10.1029/2002GB001895.

Herr, F. L. and Barger, W. R. 1978. Molecular hydrogen in the near-surface atmosphere and dissolved in waters of the tropical North Atlantic. *J. Geophys. Res.* **83**, 6199–6205.

Holton, J. R. 1990. On the global exchange of mass between the stratosphere and the troposphere. *J. Atmos. Sci.* **47**, 392–395.

Hurst, D. F., Bakwin, P. S., Zhoa, C., Davis, K. J. and Teclaw, R. M. 1996. Landscape-scale surface fluxes of methane and hydrogen in a North American boreal lowland and wetland boreal forest. *EOS, Trans. Am. Geophys. Un.* **77** (Fall Meet. Suppl.), F124–F125.

Hurst, D. F., Dutton, G. S., Romashkin, P. A., Wamsley, P. R., Moore, F. L. and co-authors. 1999. Closure of the total hydrogen budget of the northern extratropical lower stratosphere. *J. Geophys. Res.* **104**, 8191–8200.

Intergovernmental Panel on Climatic Change (IPCC) 1995. *Climate Change 1995*, Cambridge University Press, Cambridge, UK.

Intergovernmental Panel on Climatic Change (IPCC) 2008. *Climate Change 2007*. Cambridge University Press, Cambridge, UK.

International Energy Agency/Standing Group on Long-term Cooperation (IEA/SLT) 2003. *Moving to a Hydrogen Economy: Dreams and Realities*. International Energy Agency, Paris, France.

Khalil, M. A. K. and Rasmussen, R. A. 1990. Global increase of atmospheric molecular-hydrogen. *Nature* **347**, 743–745.

Koppmann, R., ed. 2007. *Volatile Organic Compounds in the Atmosphere*. Blackwell Publishing Ltd, Oxford.

Krol, M. and Lelieveld, J. 2003. Can the variability in tropospheric OH be deduced from measurements of 1,1,1-trichloroethane (methyl chloroform)? *J. Geophys. Res.* **108**, 4125, doi:10.1029/2002JD002423.

Lal, D. 2002. Cosmogenic radionuclides. In: *Encyclopedia of Atmospheric Sciences* Vol. 5 (eds. J. Holton, J. Pyle and J. A. Curry). Academic Press, 1892–1900.

Lallo, M., Aalto, T., Laurila, T. and Hatakka, J. 2006. Measurements of H_2 Deposition to Forest Soil in Southern Finland. In: *Proceedings of 2nd HyCARE meeting* (eds. M. G. Schultz and M. Schwoon). Laxenburg, Austria, 19–20 Dec. 2005, pp. 14–16.

Langenfelds, R. L., Francey, R. J., Pak, B. C., Steele, L. P., Lloyed, J. and co-authors. 2002. Interannual growth rate variations of atmospheric CO_2 and its $\delta^{13}C$, H_2, CH_4, and CO between 1992 and 1999 linked to biomass burning. *Global Biogeochem. Cycles* **16**, 1048, doi:10.1029/2001GB001466.

Liebl, K. H. and Seiler, W. 1976. *CO and H_2 Destruction at the Soil Surface in Production and Utilisation of Gases* (eds. H. G. Schlegel, G. Gottschalk and N. Pfenning). E. Goltze KG, Göttingen, Germany, pp. 215–229.

Lies, K.-H. 1988. Nonlimited automotive exhaust components (Nicht limitierte Automobil-Abgaskomponenten). *Report*, Volkswagen AG, Wolfsburg, Germany.

Lobert, J. M., Keene, W. C., Logan, J. A. and Yevich, R. 1999. Global chlorine emissions from biomass burning: reactive chlorine emissions inventory. *J. Geophys. Res.* **104**, 8373–8389.

Luo, Y., Sternberg, L., Suda, S., Kmazawa, S. and Mitsui, A. 1991. Extremely low D/H ratios of photoproduced hydrogen by cyanobacteria. *Plant Cell Physiol.* **32**, 897–900.

Mar, K. A., McCarthy, M. C., Connell, P. and Boering, K. A. 2007. Modeling the photochemical origins of the extreme deuterium enrichment in stratospheric H_2. *J. Geophys. Res.* **112**, D19302, doi:1029/2006JD007403.

Martell, E. A. 1963. On the inventory of artificial tritium and its occurrence in atmospheric methane. *J. Geophys. Res.* **68**, 3759–3769.

Martell, E. A. and Ehhalt, D. H. 1974. Hydrogen and carbon compounds in the upper stratosphere and lower mesosphere. In: *Proceedings of International Conference on structure, composition, and general circulation of the upper and lower atmospheres and possible anthropogenic perturbations*, Melbourne, Australia, 14–15 January 1974, pp. 223–228.

Mason, A. S. 1977. Atmospheric HT and HTO, 4: estimation of atmospheric hydrogen residence time from interhemispheric tritium gas transport. *J. Geophys. Res.* **82**, 5913–5916.

McLearn, N. and Dong, Z. M. 2002. Microbial nature of the hydrogen-oxidizing agent in hydrogen-treated soil. *Biol. Fertil. Soils* **35**, 465–469.

Millet, B. M., Jacob, D. J., Turquety, S., Hudman, R. C., Wu, S. and co-authors. 2006. Formaldehyde distribution over North America: implications for satellite retrieval of formaldehyde columns and isoprene emission. *J. Geophys. Res.* **111**, D24S02, doi:1029/2005JD006853.

Miyoshi, A., Hatakeyama, S. and Washida, N. 1994. OH radical initiated photo-oxidation of isoprene: an estimate of global CO production. *J. Geophys. Res.* **99**, 18 779–18 787.

Moate, P. J., Clarke, T., Davis, L. H. and Laby, R. H. 1997. Rumen gases and bloat in grazing dairy cows. *J. Agricult. Sci.* **129**, 459–469, doi:10.1017/S00221859697004930.

Montzka, S. A., Spivakovsky, C. M., Butler, J. H., Elkins, J. W., Lock, L. T. and co-author. 2000. New observational constraints for atmospheric hydroxyl on global and hemispheric scales. *Science* **288**, 500–503.

Müller, J.-F. and Stavrakou, T. 2005. Inversion of CO and NO_x emissions using the adjoint of the IMAGES model. *Atmos. Chem. Phys.* **5**, 1157–1186.

Nilsson, E. J. K., Johnson, M. S., Taketani, F., Matsumi, Y., Hurley, M. D. and co-author. 2007. Atmospheric deuterium fractionation: HCHO and HCDO yields in the $CH_2DO + O_2$ reaction. *Atmos. Chem. Phys.* **7**, 5873–5881.

Novelli, P. C., Lang, P. M., Masarie, K. A., Hurst, D. F., Myers, R. and co-authors. 1999. Molecular hydrogen in the troposphere: global distribution and budget. *J. Geophys. Res.* **104**, 30 427–30 444.

Olivier, J. G. J., Bloos, J. P. J., Berdowski, J. J. M., Visschedijk, A. J. H. and co-authors. 1999. A 1990 global emission inventory of anthropogenic sources of carbon monoxide on $1^\circ \times 1^\circ$ developed in the framework of EDGAR/GEIA. *Chemosphere Global Change Sci.* **1**, 1–17, doi:10.1016/S1465-9972(99)00019-7.

Östlund, G. and Mason, A. S. 1974. Atmospheric HT and HTO, 1: experimental procedures and tropospheric data 1968–72. *Tellus* **26**, 91–102.

Pak, B. C. 2000. Vertical structure of atmospheric trace gases over southeast Australia. Thesis. University of Melbourne, Australia, 273pp. Available at the Australian Digital Theses Project at http://dtl.unimelb.edu.au/.

Palmer, P. M., Abbot, D. S., Fu, T.-M., Jacob, D. J., Chance, K. and co-authors. 2006. Quantifying the seasonal and innterannual variability of North American isoprene emissions using satellite observations of the formaldehyde column. *J. Geophys. Res.* **111**, D12315, doi:10.1029/2005JD006689.

Paneth, F. A. 1937. The chemical composition of the atmosphere. *Q. J. R. Meteorol. Soc.* **63**, 433–438.

Prather, M. J. 2003. An environmental experiment with H_2? *Science* **302**, 581–582.

Prather, M. and Spivakovsky, C. M. 1990. Tropospheric OH and the lifetimes of hydrochlorofluoromethanes. *J. Geophys. Res.* **95**, 18 723–18 729.

Prather, M., Ehhalt, D., Dentener, F., Derwent, R., Dlugokencky, E. and co-authors. 2001. Atmospheric chemistry and greenhouse gases. In: *Climate Change 2001: The Scientific Basis, Contribution of Working Group I to the Third Assessment Report of the Intergovernmental Panel on Climate Channge* (eds. J. T. Houghton, Y. Ding, D. J. Griggs, M. Noguer, P. J. van der Linden and co-editors). Cambridge University Press, Cambridge, UK and New York, USA.

Price, H., Jaegle, L., Rice, A., Quay, P., Novelli, P. C. and co-authors. 2007. Global budget of molecular hydrogen and its deuterium content: constraints from ground station, cruise, and aircraft observations. *J. Geophys Res.* **112**, D22108, doi:10.1029/2006JD008152.

Prinn, R. G., Weiss, R. F., Miller, B. R., Huang, J., Alyea, F. N. and co-authors. 1995. Atmospheric trends and lifetime of CH_3CCl_3 and global OH concentrations. *Science* **269**, 187–192.

Prinn, R. G., Huang, J., Weiss, R. F., Cunnold, D. M., Fraser, P. J. and co-authors. 2001. Evidence for substantial variations of atmospheric hydroxyl radicals in the past two decades. *Science* **292**, 1882–1888.

Prinn, R. G., Huang, J., Weiss, R. F., Cunnold, D. M., Fraser, P. J. and co-authors. 2005. Evidence for variability of atmospheric hydroxyl radicals over the past quarter century. *Geophys. Res. Lett.* **32**, L07809, doi:10.1029/2004GL02228.

Quay, P., Stutsman, J., Wilbur, D., Snover, A., Dlugokencky, E. and co-authors. 1999. The isotopic composition of atmospheric methane. *Global Biogeochem.Cycles* **13**, 445–461.

Rahn, J., Eiler, J. M., Kitchen, N., Fessenden, J. E. and Randerson, J. T. 2002a. Concentration and dD of molecular hydrogen in boreal forests: ecosystem scale systematics of atmospheric H_2. *Geophys. Res. Lett.* **29**, doi:101029/2002GL015118.

Rahn, T., Kitchen, N. and Eiler, J. 2002b. D/H ratios of atmospheric H_2 in urban air: results using new methods for analysis of nano-molar H_2 samples. *Geochim. Cosmochim. Acta* **66**, 2575–2481.

Rahn, T., Eiler, J. M., Boering, K. A., Wennberg, P. O., McCarthy, M. C. and co-author. 2003. Extreme deuterium enrichment in stratospheric hydrogen and the global atmospheric budget of H_2. *Nature* **424**, 918–921.

Rhee, T. S., Brenninkmeijer, C. A. M. and Röckmann, T. 2006a. The overwhelming role of soils in the global atmospheric hydrogen cycle. *Atmos. Chem. Phys.* **6**, 1611–1625.

Rhee, T. S., Brenninkmeijer, C. A. M., Braß, M. and Brühl, C. 2006b. Isotopic composition of H_2 from CH_4 oxidation in the stratosphere and the troposphere. *J. Geophys, Res.* **111**, D23303, doi:10.1029/2005JD006760.

Rhee, T. S., Brenninkmeijer, C. A. M. and Röckmann, T. 2007. Hydrogen isotope fractionation in the photolysis of formaldehyde. *Atmos. Chem. Phys. Discuss.* **7**, 12 715–12 750.

Röckmann, T., Rhee, T. S., Engel, A. 2003. Heavy hydrogen in the stratosphere. *Atmos. Chem. Phys.* **3**, 2015–2023.

Rohs, S., Schiller, C., Riese, M., Engel, A., Schmidt, U. and co-authors. 2006. Long-term changes of methane and hydrogen in the stratosphere in the period 1978–3003 and their impact on the abundance of stratospheric water vapor. *J. Geophys. Res.* **111**, D14315, doi:1029/2005JD006877.

Sander, S. P., Friedl, R. R., Golden, D. M., Kurylo, M. J., Moortgat, G. K. and co-authors. 2006. *Chemical kinetics and photochemical data for use in atmospheric studies*. *Evaluation No. 15*. JPL Publication 06–2. NASA/Jet Propulsion Laboratory, Pasadena, CA.

Sanderson, M. G. 1996. Biomass of termites and their emissions of methane and carbon dioxide: a global data base. *Global Biogeochem. Cycles* **10**, 543–557.

Sanderson, M. G., Collins, W. J., Derwent, R. G. and Johnson, C. E. 2003. Simulation of global hydrogen levels using a Lagrangian three-dimensional model. *J. Atmos. Chem.* **46**, 15–28.

Sanhueza, E., Dong, Y., Scharffe, D., Lobert, J. M. and Crutzen, P. J. 1998. Carbon monoxide uptake by temperate forest soils: the effects of leaves and humus layers. *Tellus* **50B**, 51–58.

Saunders, S. M., Jenkin, M. E., Derwent, R. G. and Pilling, M. J. 2003. Protocol for the development of the Master Chemical Mechanism, MCM v3, Part A: troposheric degradation of non-aromatic volatile organic compounds. *Atmos. Chem. Phys.* **3**, 161–180.

Schiegl, W. E. and Vogel, J. C. 1970. Deuterium content of organic matter. *Earth Planet. Sci. Lett.* **7**, 307–313.

Schmidt, U. 1974. Molecular hydrogen in atmosphere. *Tellus* **26**, 78–90.

Schmidt, U. 1978. The latitudinal and vertical distribution of molecular hydrogen in the troposphere. *J. Geophys. Res.* **83**, 941–946.

Schmidt, U. and Seiler, W. 1970. A new method for recording molecular hydrogen in atmospheric air. *J. Geophys. Res.* **75/9**, 1713–1716.

Schmidt, U. and Wetter, T. 2002. Tropospheric chemistry and composition: H_2. In: *Encyclopedia of Atmospheric Sciences* Vol. 6 (eds. J. Holton, J. Pyle and J. A. Curry). Academic Press, London, 2397–2402.

Schmidt, U., Kulessa, G. and Röth, E. P. 1980. The atmospheric H_2 cycle. In: *Proceedings of the NATO Advanced Study Institute on Atmospheric Ozone* (ed. A. C. Aikin). U.S. Department of Transportation, Report No. FAA-EE-80-20. Aldeias das Acoteias, Portugal, pp. 307–322.

Scholz, T. G., Ehhalt, D. H., Heidt, L. E. and Martell, E. A. 1970. Water vapor, molecular hydrogen, methane, and tritium concentrations near the stratopause. *J. Geophys. Res.* **75**, 3049–3054.

Schuler, S. and Conrad, R. 1990. Soils contain two different activities for oxidation of hydrogen. *FEMS Microbiol. Ecol.* **73**, 77–84.

Schuler, S. and Conrad, R. 1991. Hydrogen oxidation activities in soil as influenced by pH, temperature, moisture, and season. *Biol. Fertility Soils* **12**, 127–130.

Schultz, M. G., Diehl, T., Brasseur, G. P. and Zittel, W. 2003. Air pollution and climate-forcing impacts of a global hydrogen economy. *Science* **302**, 624–627.

Schultz, M. G., Heil, A., Hoelzemann, J. J., Spessa, A., Thonicke, K. and co-author. 2008. Global wildland fire emissions from 1960 to 2000. *Global Biogeochem. Cycles* **22**, GB2002, doi:10.1029/2007GB003031.

Seiler, W. and Conrad, R. 1987. Contribution of tropical ecosystems to the global budgets of trace gases, especially CH_4, H_2, CO and N_2O. In: *The Geophysiology of Amazonia* (ed. R. E. Dickinson). John Wiley & Sons, New York, pp. 133–157.

Seiler, W. and Schmidt, U. 1974. Dissolved nonconservative gases in seawater. In: *The Sea* Vol. 5: *Marine Chemistry* (ed. E. D. Goldberg). J. Wiley & Sons, Inc., New York, 219–243.

Seiler, W. and Zankl, H. 1975. The trace gases CO and H_2 above Munich (Die Spurengase CO und H_2 über München). *Umschau* **75**, 735–736.

Seiler, W., Müller, F. and Oeser, H. 1978. Vertical distribution of chlorofluoromethanes in the upper troposphere and lower stratosphere. *Pure Appl. Geophys.* **116**, 554–566.

Simmonds, P. G., Derwent, R. G., O'Doherty, S., Ryall, D. B., Steele, L. P. and co-authors. 2000. Continuous high-frequency observations of hydrogen at the Mace Head Baseline – atmospheric monitoring station over the 1994–1998 period. *J. Geophys. Res.* **105/D10**, 12 105–12 121.

Singh, H. B., Salas, L. J., Chatfield, R. B., Czech, E., Fried, A. and co-authors. 2004. Analysis of the atmospheric distribution, sources, and sinks of oxygenated volatile orcganic chemicals based on measurements over the Pacific during TRACE-P. *J. Geophys. Res.* **109**, D15S07, doi:10.1029/2003JD003883.

Smith-Downey, N. V., Randerson, J. T. and Eiler, J. M. 2006. Temperature and moisture dependence of soil H_2 uptake measured in the laboratory. *Geophys. Res. Lett.* **33**, L14813, doi:10.1029/2006GL026749.

Smolenski, W. J. and Robinson, J. A. 1988. In situ rumen hydrogen concentrations in steers fed eight times daily, measured using a mercury reduction detector. *FEMS Microbiol. Ecol.* **53**, 95–100.

Sone, Y., Tanida, S., Matsubara, K., Kojima, Y., Kato, N. and co-authors. 2000. Everyday breath hydrogen excretion profile in Japanese young female students. *J. Physiol. Anthropol.* **19**, 229–237.

Spivakovsky, C. M., Logan, J. A., Montzka, S. A., Balkanski, Y. J., Foreman-Fowler, M. and co-authors. 2000. Three-dimensional climatological distribution of tropospheric OH: update and evaluation. *J. Geophys. Res.* **105**, 8931–8980.

Steinbacher, M., Fischer, A., Vollmer, M. K., Buchmann, B., Reimann, S. and co-authors. 2007. Perennial observations of molecular hydrogen (H_2) at a suburban site in Switzerland. *Atmos. Env.* **41**, 2111–2124.

Steiner, A. H. and Goldstein, A. L. 2007. Biogenic VOCs, In: *Volatile Organic Compounds in the Atmosphere* (ed. R. Koppmann). Blackwell Publishing Ltd, Oxford, 82–128.

Sugimoto, A., Inoue, T., Tayasu, I., Miller, L., Takeichi, S. and co-authors. 1998. Methane and hydrogen production in a termite-symbiont system. *Ecol. Res.* **13**, 241–257.

Taatjes, C. A. 1999. Infrared frequency-modulation measurements of absolute rate coefficients for Cl + HD -> HCl(DCl) + D(H) between 295 and 700K. *Chem. Phys. Lett.* **306**, 33–40.

Talukdar, R. K. and Ravishankara, A. R. 1996. Rate coefficients for $O(^1D)$ + H_2, D_2, HD reactions and H atom yield in $O(^1D)$ + HD reaction. *Chem. Phys. Lett.* **243**, 177–183.

Talukdar, R. K., Gierczak, T., Goldfarb, L., Rudich, Y., Madhava Rao, B. S. and co-authors. 1996. Kinetics of hydroxyl radical reaction with isotopically labelled hydrogen. *J. Phys. Chem.* **100**, 3037–3043.

Tie, X., Guenther, A. and Holland, E. 2003. Biogenic methanol and its impacts on tropospheric oxidants. *Geophys. Res. Lett.* **30**, 1881, doi:1029/2003GL017167.

Trenberth, K. F. and Guillemot, G. J. 1994. The total mass of the atmosphere. *J. Geophys. Res.* **99**, 23 079–23 088.

Tromp, T. K., Shia, R.-L., Allen, M., Eiler, J. M. and Yung, Y. L. 2003. Potential environmental impact of a hydrogen economy on the stratosphere. *Science* **300**, 1740–1742.

Vollmer, M. K., Juergens, N., Steinbacher, M., Reimann, S., Weilenmann, M. and co-authors. 2007. Road vehicle emissions of molecular hydrogen (H_2) from a tunnel study. *Atmos. Env.* **41**, 8355–8369.

Warneck, P. 1988. *Chemistry of the Natural Atmosphere*. Academic Press Inc., San Diego, CA.

Warwick, N. J., Bekki, S., Nisbet, E. G. and Pyle, J. A. 2004. Impact of a hydrogen economy on the stratosphere and troposphere studied in a 2-D model. *Geophys. Res. Lett.* **31**, L05107, doi:10.1029/2003GL019224.

Williams, R. T. and Bainbridge, A. E. 1973. Dissolved CO, CH_4, and H_2 in the Southern Ocean. *J. Geophys. Res.* **78**, 2691–2694.

Wittrock, F., Richter, A., Oetjen, H., Burrows, J. P., Kanakidou, M. and co-authors. 2006. Simultaneous global observations of glyoxal and formaldehyde from space. *Geophys. Res. Lett.* **33**, L16804, doi:10.1029/2006GL026310.

Xiao, X., Prinn, R. G., Simmonds, P. G., Steele, L. P., Novelli, P. C. and co-authors. 2007. Optimal estimation of the soil uptake of molecular hydrogen from the Advanced Global Atmospheric Gases Experiments and other measurements. *J. Geophys. Res.* **112**, D07303, doi:10.1029/2006JD007241.

Yevich, R. and Logan, J. A. 2003. An assessment of biofuel use and burning of agricultural waste in the developing world. *Global Biogeochem. Cycles* **17**, 1095, doi:10.1029/2002GB001952.

Yonemura, S., Kawashima, S. and Tsuruta, H. 1999. Continuous measurements of CO and H_2 deposition velocities onto an andisol: uptake control by soil moisture. *Tellus* **51B**, 688–700.

Yonemura, S., Yokozawa, M., Kawashima, S. and Tsuruta, H. 2000a. Model analysis of the influence of gas diffusivity in soil on CO and H_2 uptake. *Tellus* **52B**, 919–933.

Yonemura, S., Kawashima, S. and Tsuruta, H. 2000b. Carbon monoxide, hydrogen, and methane uptake by soils in a temperate arable field and a forest. *J. Geophys. Res.* **105**, 14 347–14 362.

Zander, R., Demoulin, Ph., Ehhalt, D. H., Schmidt, U. and Rinsland, C. P. 1989. Secular increase of the total vertical column abundance of carbon monoxide above central Europe since 1950. *J. Geophys. Res.* **94**, 11 021–11 028.

Zellner, R., Wagner, G. and Himme, B. 1980. H_2 formation in the reaction of $O(^1D)$ with H_2O. *J. Phys. Chem.* **84**, 3196–3198.

Zimmerman, P. R., Greenberg, J. P., Wandiga, S. O. and Crutzen, P. J. 1982. Termites: a potentially large source of atmospheric methane, carbon dioxide, and molecular hydrogen. *Science* **218**, 563–565.

Zöger, M., Engel, A., McKenna, D. S., Schiller, C., Schmidt, U. and coauthors. 1999. Balloon-borne in situ measurements of stratospheric H_2O, CH_4, and H_2 at midlatitudes. *J. Geophys. Res.* **104**, 1817–1825.